Accepted Manuscript

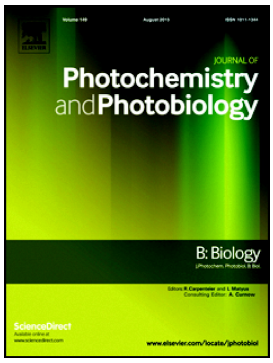

Synthesis, photodynamic activity, and quantitative structure-activity relationship modelling of a series of BODIPYs

Enrico Caruso, Marzia Gariboldi, Alessandro Sangion, Paola Gramatica, Stefano Banfi

PII: S1011-1344(16)30985-X
DOI: doi: 10.1016/j.jphotobiol.2017.01.012
Reference: JPB 10713

To appear in: *Journal of Photochemistry & Photobiology, B: Biology*

Received date: 2 November 2016
Accepted date: 9 January 2017

Please cite this article as: Enrico Caruso, Marzia Gariboldi, Alessandro Sangion, Paola Gramatica, Stefano Banfi , Synthesis, photodynamic activity, and quantitative structure-activity relationship modelling of a series of BODIPYs. The address for the corresponding author was captured as affiliation for all authors. Please check if appropriate. Jpb(2017), doi: 10.1016/j.jphotobiol.2017.01.012

Synthesis, Photodynamic activity, and Quantitative Structure-Activity Relationship Modeling of a series of BODIPYs

Enrico Caruso[1], Marzia Gariboldi[1], Alessandro Sangion[2], Paola Gramatica[2], Stefano Banfi[1]*

1 Department of Biotechnology and Life Sciences (DBSV). University of Insubria, Via J.H. Dunant 3, 21100 Varese (VA), Italy.

2 Department of Theoretical and Applied Sciences (DiSTA), University of Insubria, Via J.H. Dunant 3, 21100 Varese (VA), Italy.

*To whom correspondence should be addressed. Phone: +39-0332-421550. Fax: +39-0332-421554. E-mail: enrico.caruso@uninsubria.it

Abstract

Here we report the synthesis of eleven new BODIPYs (**14** – **24**) characterized by the presence of an aromatic ring on the 8 (*meso*) position and of iodine atoms on the pyrrolic 2,6 positions. These molecules, together with twelve BODIPYs already reported by us (**1** – **12**), represent a large panel of BODIPYs showing different atoms or groups as substituent of the aromatic moiety. Two physico-chemical features ($^1O_2$ generation rate and lipophilicity), which can play a fundamental role in the outcome as photosensitizers, have been studied. The *in vitro* photo-induced cell-killing efficacy of 23 PSs was studied on the SKOV3 cell line treating the cells for 24 h in the dark then irradiating for 2 h with a green LED device (fluence 25.2 J/cm^2). The cell-killing efficacy was assessed with the MTT test and compared with that one of *meso* un-substituted compound (**13**). In order to understand the possible effect of the substituents, a predictive quantitative structure-activity relationship (QSAR) regression model, based on theoretical holistic molecular descriptors, was developed. The results clearly indicate that the presence of an aromatic ring is fundamental for an excellent photodynamic response, whereas the electronic effects and the position of the substituents on the aromatic ring do not influence the photodynamic efficacy.

Keywords: Photodynamic Therapy, BODIPY, tumor cells, singlet oxygen, QSAR

Introduction

Photodynamic therapy (PDT) is a light-based therapeutic approach used for the treatment of various diseases, including precancerous skin pathologies and localized solid tumors. PDT involves the administration of a photosensitizer (PS), topically applied directly on the diseased tissue or intravenously administered. After the appropriate time of incubation, the effective step of PDT is the area-selective irradiation with visible light to induce the electronic excitation of the PS.

In the presence of adequate concentrations of molecular oxygen in the tissue, the light activated PS transfers its energy to molecular oxygen, leading to the generation of reactive oxygen species (ROS) that are responsible for PDT-based cell-killing which could lead to tumor ablation [1,2].

Porfimer sodium (Photofrin®) a purified form of hematoporphyrin derivative consisting of a mixture of porphyrins, was the first PS approved by the US Food and Drug Administration (FDA). Despite the encouraging results in the treatment of a variety of cancers, including lung, esophageal, stomach and bladder adenocarcinoma, porfimer sodium is not devoid of drawbacks and limits, such as weak absorption in the red region of the visible spectrum, a poor selectivity between tumours and normal tissues and a long lasting skin phototoxicity [3,4].

Most of the drug-development efforts aimed at overcoming these problems have resulted in novel "second generation" PS with improved properties. Some second-generation PSs, such as verteporfin (Visudine®), temoporfin (mTHPC, Foscan®), chlorophyll-*a* derivative (Radachlorin®), Pd-bacteriopheophorbide-*a* derivative (Tookad®) and pyropheophorbide-*a* derivative (HPPH), belong to the cyclic tetrapyrrolic class of molecules [5], exhibiting relatively high affinity for tumour tissues [6], low intrinsic toxicity and intense absorption properties in the therapeutic window of the visible electromagnetic spectrum (600 – 700 nm). On the other hand, the synthesis of the PSs from chlorophyll is quite demanding because of the instability of the natural starting molecule.

An alternative class of non-porphyrin compounds, based on a difluoro-boradiazaindacenes skeleton, also known as boron-dipyrromethenes (BODIPY), has emerged over the last decade. BODIPY derivatives proved to be useful fluorophores in many applications, such as fluorescent labelling of

biomolecules, material for energy transfer cassettes and fluorescent chemosensors for detection of ionic species [7-11].

BODIPYs show many characteristics including: easy synthetic pathway, tuneable hydrophilic/hydrophobic character [12-14], high extinction coefficients in the visible region (relatively unaffected by environmental conditions) [15,16], partial resistance to photobleaching [17] and high quantum efficiencies of fluorescence (Φ_{fl}) [18]. The last two features exert a negative effect whenever BODIPYs are envisaged as PS; actually, while photodynamic activity may benefit from a long half-life of the photoactivatable molecules, this property might be associated with persistent skin photosensitization. Furthermore, although a high quantum yields of fluorescence is fundamental when BODIPYs are exploited as biological probes, the light emission should be limited when BODIPYs are engineered for PDT. To this purpose, fluorescence must be depressed, thus avoiding the energy dispersion from the singlet excited PS, favouring the formation of a PS triplet excited state from which occurs a process useful for the production of cell toxic reactive oxygen species.

As far as it concerns the availability of these PSs, the straightforward "one pot" synthesis is a practical advantage favouring the development of these molecules that can be isolated in fairly good yields after a single chromatographic purification.

Here we report the synthesis of a panel of fully characterized BODIPY featuring an aromatic ring on the *meso (8)* position, characterized by the presence of different substituents. These new molecules, together with thirteen BODIPYs previously synthesized by us [19], were studied to determine the singlet oxygen ($^1O_2$) production rates, the fluorescent quantum yield and, finally, the relative degree of lipophilicity. The photodynamic activity of these compounds, all characterized by intense absorbance in the 495 – 535 nm range, has been assessed on the ovarian carcinoma (SKOV3) cell line, following irradiation with a low energy green LED light. Quantitative structure-activity relationship (QSAR) analysis was also performed on the whole set of the BODIPYs here reported.

Experimental section

General.

^{1}H and ^{13}C NMR spectra were recorded on a Bruker 400 MHz spectrometer in $CDCl_3$ or [d6] DMSO; chemical shifts are expressed in ppm relative to chloroform (7.28) and are reported as s (singlet), bs (broad singlet), d (doublet), t (triplet) and m (multiplet). Mass spectrometric measurements were performed on a Bruker Esquire 3000 Plus. Elemental analyses were performed on a ThermoQuest NA 2100, C, H, N analyzer, equipped with an electronic mass flow control and thermal conductivity detector. Merck 60 F254 silica gel precoated sheets (0.2 mm thick) were used for analytical thin-layer chromatography (TLC). Silica gel 60 (70-230 mesh, Merck) was used for column chromatography. Aromatic aldehydes and 2,4-dimethylpyrrole were commercial products (Sigma-Aldrich) and used as received. Dichloromethane used for BODIPY synthesis was distilled from $CaCl_2$ directly into the reaction flask. HPLC analyses were conducted with an Agilent 1100 Series instrument coupled with a diode array detector. The instrument was fitted with a 250×4.6 mm column (Supelco, Ascentis) packed with C-18 reversed-phase particles (5 μm), operating with an isocratic elution of MeCN at 0.5 mL/min. The green LED array is composed of 12×3 W diodes distributed on an 11 cm diameter disk, and equipped with a heat sinker. The emitted light is characterized by a lambda max (λ_{max}) at 525 nm (fluence rate 3.5 x 10^{-3} W/cm^2, light energy density, or fluence, 25.2 J/cm^2) and a width at half maximum of 70 nm. The electric supply was ensured by a 50 W current transformer. This array was placed above the plate at such a distance as to produce a homogeneous area of irradiation with a fluence rate (irradiance) of 7.52×10^{-5} W/cm^2 at 525 nm (λ of maximum emission), as determined with a LI-COR 1800 spectroradiometer.

Synthesis.

4,4-difluoro-2,6-diiodo-1,3,5,7-tetramethyl-8-(3'-iodo-4',5'-dimethoxyphenyl)-4-bora-3a,4adiaza-s-indacene (**1**); 4,4-difluoro-2,6-diiodo-1,3,5,7-tetramethyl-8-(4'-methoxyphenyl)-4-bora-3a,4adiaza-s-indacene (**2**); 4,4-difluoro-2,6-diiodo-1,3,5,7-tetramethyl-8-(3'-methoxyphenyl)-4-bora-3a,4adiaza-s-indacene (**3**); 4,4-difluoro-2,6-diiodo-1,3,5,7-tetramethyl-8-(4'-hydroxy-3',5'-

diiodophenyl)-4-bora-3a,4adiaza-s-indacene (**4**); 4,4-difluoro-2,6-diiodo-1,3,5,7-tetramethyl-8-(3'-hydroxy-4'-iodophenyl)-4-bora-3a,4adiaza-s-indacene (**5**); 4,4-difluoro-2,6-diiodo-1,3,5,7-tetramethyl-8-(4'-methoxynaphthalene)-4-bora-3a,4adiaza-s-indacene (**6**); 4,4-difluoro-2,6-diiodo-1,3,5,7-tetramethyl-8-(4',7'-dimethoxynaphthalene)-4-bora-3a,4adiaza-s-indacene (**7**); 4,4-difluoro-2,6-diiodo-1,3,5,7-tetramethyl-8-(2',6'-dichlorophenyl)-4-bora-3a,4adiaza-s-indacene (**8**); 4,4-difluoro-2,6-diiodo-1,3,5,7-tetramethyl-8-(2',3',4',5',6'-pentafluorophenyl)-4-bora-3a,4adiaza-s-indacene (**9**); 4,4-difluoro-2,6-diiodo-1,3,5,7-tetramethyl-8-(2',3',5',6'-tetrafluoro-3'-[(4''-methoxybenzyl)sulfanyl]phenyl)-4-bora-3a,4adiaza-s-indacene (**10**); 4,4-difluoro-2,6-diiodo-1,3,5,7-tetramethyl-8-(4'-pyridyl)-4-bora-3a,4adiaza-s-indacene (**11**); 4,4-difluoro-2,6-diiodo-1,3,5,7-tetramethyl-8-(3'-pyridyl)-4-bora-3a,4adiaza-s-indacene (**12**); 4,4-difluoro-2,6-diiodo-1,3,5,7-tetramethyl-4-bora-3a,4adiaza-s-indacene (**13**) were synthesized as previously described [19].

4,4-difluoro-2,6-diiodo-1,3,5,7-tetramethyl-8-(2'-chloro-6'-nitrophenyl)-4-bora-3a,4adiaza-s-indacene (14). To a 30 mL solution of 2-chloro-6-nitrobenzaldehyde (213 mg, 1.15 mmol) and 2,4-dimethylpyrrole (260 µL, 2.53 mmol) in dry CH_2Cl_2, kept under N_2 atmosphere, were added ten drops of TFA. The solution was then stirred at RT for the time necessary to obtain the complete consumption of the aldehyde (from 6 to 12 h) as determined by TLC analysis. Thereafter the oxidation of the dipyrrolylmethane to dipyrrolylmethene was carried out, in the same flask, by the addition of DDQ (391.6 mg, 1.725 mmol) and the mixture was stirred for 30 min. The last step of the BODIPY synthesis requires the addition of Et_3N (3 mL) and $BF_3{\cdot}OEt_2$ (3 mL) thus producing the desired borinated final compound. This step requires about 12 h, then the organic layer was washed two times with water, two time with a HCl 1 M solution and then other three times with water. The organic solution was dried over Na_2SO_4, filtered and evaporated to dryness. The raw material was purified by column chromatography (SiO_2 50 g, petroleum ether-CH_2Cl_2, 3:7) affording 197 mg (0.49 mmol, yield: 42.6%) of **14a** in the form of orange needles, mp = 190 °C. UV-vis$_{(CH_3CN)}$: 513 nm (ε=63600); Φ_{fluo} (526 nm): 0.68; ^{1}H NMR ($CDCl_3$) δ 1.46 (s, 6H, 2×CH_3),

2.59 (s, 6H, 2×CH_3), 6.03 (s, 2H), 7.66 (t, 1H, J = 12 Hz), 7.85 (d, 1H, J = 12 Hz), 8.03 (d, 1H, J = 12 Hz).

The corresponding 2,6-diiodo compound (**14**) was synthesised treating with I_2 (231.5 mg, 0.912 mmol) and HIO_3 (160.4 mg, 0.912 mmol) an EtOH solution of compound **14a** (184 mg, 0.456 mmol). This mixture was stirred for 15–18 h at RT, then washed with water and extracted three times with CH_2Cl_2; the organic phase was dried over Na_2SO_4 and evaporated to dryness. The crude product was purified by column chromatography (SiO_2 40 g, petroleum ether-CH_2Cl_2, 1:1) affording 79 mg (0.12 mmol; yield: 26.3%, overall yield: 10%) of **14** as red needles, mp > 300 °C; EA: calcd for $C_{19}H_{15}BClF_2I_2N_3O_2$ C, 34.82; H, 2.31; N, 6.41; found: C, 35.01; H, 2.32; N, 6.45; UV-vis$_{(CH_3CN)}$: 548 nm (ε=49700); Φ_{fluo} (555 nm): 0.02; ^{1}H NMR ($CDCl_3$) δ 1.47 (s, 6H, 2×CH_3), 2.69 (s, 6H, 2×CH_3), 7.73 (t, 1H, J = 12 Hz), 7.89 (dd, 1H, J_1 = 12 Hz, J_2 = 4 Hz), 8.11 (dd, 1H); ^{13}C NMR ($CDCl_3$) δ 15.84, 16.32, 86.03, 124.39, 128.99, 130.41, 131.78, 132.99, 135.00, 139.52, 144.15, 148.15, 157.98; MS (ESI): M-1$^+$ found: 654.32 calcd for $C_{19}H_{15}BClF_2I_2N_3O_2$ 655.41; HPLC: retention time = 8’28’’ (100%); Photo-degradation t_{60}: 55%, t_{120}: 71%.

4,4-difluoro-2,6-diiodo-1,3,5,7-tetramethyl-8-(2’-methoxyphenyl)-4-bora-3^a,4adiaza-s-indacene (15). 2,4-Dimethylpyrrole (400 µL, 3.89 mmol) and 2-methoxybenzaldehyde (241 mg, 1.77 mmol) were reacted as described for compound **14a**. The raw material was purified by column chromatography (SiO_2 45 g, petroleum CH_2Cl_2-MeOH, 95:5) affording 55 mg (0.16 mmol; yield: 9.0%) of orange needles. mp = 200 °C. UV-vis$_{(CH_3CN)}$: 500 nm (ε=95000); Φ_{fluo} (529 nm): 0.61; ^{1}H NMR ($CDCl_3$) δ 1.45 (s, 6H, 2×CH_3), 2.57 (s, 6H, 2×CH_3), 3.79 (s, 3H, OCH_3), 5.98 (s, 2H), 7.01 (d, 1H, J = 8 Hz), 7.11 (m, 2H), 7.47 (m, 1H).

Compound **15a** (49.6 mg, 0.140 mmol) was iodinated in the presence of I_2 (71 mg, 0.280 mmol) and HIO_3 (49.2 mg, 0.280 mmol) as described for compound **14**. The crude product was purified by column chromatography (SiO_2 27 g, petroleum ether-$CHCl_3$, 2:8) affording 56 mg (0.09 mmol; yield: 64.3%) of **15** as red needles, mp > 300 °C; EA: calcd for $C_{20}H_{19}BF_2I_2N_2O$ C, 39.64; H, 3.16; N, 4.62; found: C, 39.85; H, 3.18; N, 4.63; UV-vis$_{(CH_3CN)}$: 531 nm (ε=60400); Φ_{fluo} (559 nm): 0.03;

^{1}H NMR ($CDCl_3$) δ 1.47 (s, 6H, 2×CH_3), 2.67 (s, 6H, 2×CH_3), 3.79 (s, 3H, OCH_3), 7.03 (d, 1H, J = 8 Hz), 7.12 (m, 2H), 7.52 (m, 1H); ^{13}C NMR ($CDCl_3$) δ 16.02, 16.28, 55.69, 85.30, 111.37, 121.78, 123.55, 129.29, 131.25, 131.45, 138.91, 144.84, 156.21, 156.34; MS (ESI): M-1^{+} found: 604.88 calcd for $C_{20}H_{19}BF_2I_2N_2O$ 606.00; HPLC: retention time = 12'09'' (98.1%); Photo-degradation t_{60}: 50%, t_{120}: 71%.

4,4-difluoro-2,6-diiodo-1,3,5,7-tetramethyl-8-(4'-nitrophenyl)-4-bora-3a,4adiaza-s-indacene (16). 2,4-Dimethylpyrrole (340 µL, 3.30 mmol) and 4-nitrobenzaldehyde (226.7 mg, 1.50 mmol) were reacted as described for compound **14a**. The raw material was purified by column chromatography (SiO_2 50 g, petroleum CH_2Cl_2-petroleum ether, 6:4) affording 61 mg (0.16 mmol; yield: 11%) of orange needles. mp = 189 °C. UV-vis$_{(CH_3CN)}$: 501 nm (ε=110500); Φ_{fluo} (521 nm): 0.78; ^{1}H NMR ($CDCl_3$) δ 1.38 (s, 6H, 2×CH_3), 2.59 (s, 6H, 2×CH_3), 6.04 (s, 2H), 7.56 (d, 2H, J = 9 Hz), 8.41 (d, 2H, J = 9 Hz).

The compound **16a** (48 mg, 0.130 mmol) was treated with I_2 (66 mg, 0.260 mmol) and HIO_3 (45.7 mg, 0.260 mmol) as described for compound **14**. The crude product was purified by column chromatography (SiO_2 20 g, petroleum ether-CH_2Cl_2, 1:1) affording 50 mg (0.080 mmol; yield: 61.5%) of **16** as red needles, mp > 300 °C; EA: calcd for $C_{19}H_{16}BF_2I_2N_3O_2$ C, 36.75; H, 2.60; N, 6.77; found: C, 36.82; H, 2.60; N, 6.82; UV-vis$_{(CH_3CN)}$: 535 nm (ε=65400); Φ_{fluo} (552 nm): 0.01; ^{1}H NMR ($CDCl_3$) δ 1.40 (s, 6H, 2×CH_3), 2.69 (s, 6H, 2×CH_3), 7.55 (d, 2H, J = 9 Hz), 8.45 (d, 2H, J = 9 Hz); ^{13}C NMR ($CDCl_3$) δ 16.18, 17.35, 86.47, 124.67, 129.56, 130.54, 137.82, 141.59, 144.72, 148.64, 158.07; MS (ESI): M-1^{+} found: 620.01 calcd for $C_{19}H_{16}BF_2I_2N_3O_2$ 620.97; HPLC: retention time = 9'57'' (100%); Photo-degradation t_{60}: 57%, t_{120}: 74%.

4,4-difluoro-2,6-diiodo-1,3,5,7-tetramethyl-8-(3'-cyanophenyl)-4-bora-3a,4adiaza-s-indacene (17). 2,4-Dimethylpyrrole (340 µL, 3.30 mmol) and 3-cyanobenzaldehyde (197 mg, 1.50 mmol) were reacted as described for compound **14a**. The raw material was purified by column chromatography (SiO_2 40 g, petroleum CH_2Cl_2-petroleum ether, 6:4) affording 79 mg (0.22 mmol;

yield: 14.7%) of **17a** as an orange needles. mp = 195 °C. UV-vis$_{(CH_3CN)}$: 500 nm (ε=79000); Φ_{fluo} (519 nm): 0.68; ^{1}H NMR (CD_3OD) δ 1.38 (s, 6H, 2×CH_3), 2.58 (s, 6H, 2×CH_3), 6.03 (s, 2H), 7.60 (d, 1H, J = 10 Hz), 7.68 (m, 2H), 7.83 (d, 1H, J = 10 Hz).

The **17a** (67 mg, 0.20 mmol), I_2 (101.5 mg, 0.40 mmol) and HIO_3 (70.4 mg, 0.40 mmol) were reacted as described for compound **14**. The crude product was purified by column chromatography (SiO_2 25 g, petroleum CH_2Cl_2-petroleum ether, 6:4) affording 55 mg (0.091 mmol; yield: 45.5%) of **17** as red needles, mp > 300 °C; EA: calcd for $C_{20}H_{16}BF_2I_2N_3$ C, 39.97; H, 2.68; N, 6.99; found: C, 40.22; H, 2.67; N, 6.93; UV-vis$_{(CH_3CN)}$: 534 nm (ε=57000). Φ_{fluo} (551 nm): 0.02; ^{1}H NMR ($CDCl_3$) δ 1.40 (s, 6H, 2×CH_3), 2.68 (s, 6H, 2×CH_3), 7.58 (dt, 1H, J_1 = 3 Hz, J_2 = 15 Hz), 7.65 (t, 1H, J = 3 Hz), 7.72 (t, 1H, J = 9 Hz), 7.88 (dt, 1H, J_1 = 3 Hz, J_2 = 9 Hz); ^{13}C NMR ($CDCl_3$) δ 16.15, 17.35, 86.41, 113.99, 117.54, 130.47, 130.94, 131.65, 132.59, 133.21, 136.36, 137.49, 144.74, 158.00; MS (ESI): M+1$^+$ found: 601.95 calcd for $C_{20}H_{16}BF_2I_2N_3$ C 600.98; HPLC: retention time = 9'20'' (99.80%) Photo-degradation t_{60}: 54%, t_{120}: 72%.

4,4-difluoro-2,6-diiodo-1,3,5,7-tetramethyl-8-(2',5'-dibromophenyl)-bora-3a,4a-diaza-s-indacene (18). 2,4-Dimethylpyrrole (340 µL, 3.30 mmol) and 2,5-dibromobenzaldehyde (396 mg, 1.50 mmol) were reacted as described for compound **14a**. The raw material was purified by column chromatography (SiO_2 55 g, petroleum ether-CH_2Cl_2, 4:6) affording 95 mg (0.20 mmol; yield: 13.3%) of **18a** as an orange needles. mp = 274 °C. UV-vis$_{(CH_3CN)}$: 505 nm (ε=151000); Φ_{fluo} (524 nm): 0.80; ^{1}H NMR (CD_3OD) δ 1.50 (s, 6H, 2×CH_3), 2.58 (s, 6H, 2×CH_3), 6.04 (s, 2H), 7.50 (d, 1H, J = 12 Hz), 7.51 (s, 1H), 7.59 (d, 1H, J = 12 Hz).

The **18a** (91 mg, 0.19 mmol), I_2 (96.4 mg, 0.38 mmol) and HIO_3 (66.84 mg, 0.38 mmol) were reacted as described for compound **14**. The crude product was purified by column chromatography (SiO_2 32 g, petroleum ether-CH_2Cl_2, 4:6) affording 78 mg (0.106 mmol; yield: 55.8%) of **18** as red needles, mp > 300 °C; EA: calcd for $C_{19}H_{15}BBr_2F_2I_2N_2$ C, 31.10; H, 2.06; N, 3.82; found: C, 31.15; H, 2.06; N, 3.84; UV-vis$_{(CH_3CN)}$: 540 nm (ε=53000); Φ_{fluo} (555 nm): 0.03; ^{1}H NMR (CD_3OD) δ 1.53

(s, 6H, 2×CH_3), 2.68 (s, 6H, 2×CH_3), 7.47 (d, 1H, J = 6 Hz), 7.56 (dd, 1H, J_1 = 12 Hz, J_2 = 3 Hz), 7.62 (d, 1H, J = 12 Hz); ^{13}C NMR ($CDCl_3$) δ 16.16, 16.88, 85.79, 124.91, 125.32, 130.65, 131.13, 132.71, 133.12, 138.21, 139.52, 143.34, 157.01; MS (ESI): M-H^+ found: 730.76 calcd for $C_{19}H_{15}BBr_2F_2I_2N_2$ C 733.36; HPLC: retention time = 16'21'' (96.0%); Photo-degradation t_{60}: 49%, t_{120}: 66%.

4,4-difluoro2,6-diiodo-1,3,5,7-tetramethyl-8-[2'-(2''-hydroxyethoxy)phenyl)]-4-bora-3a,4adiaza-s-indacene (19). 2,4-Dimethylpyrrole (340 µL, 3.30 mmol) and 2-(2-hydroxyethoxy)benzaldehyde (249 mg, 1.50 mmol) were reacted as described for compound **14a**. The raw material was purified by column chromatography (SiO_2 42 g, petroleum CH_2Cl_2-MeOH, 98:2) affording 157 mg (0.409 mmol; yield: 27.3%) of **19a** as an orange needles. mp > 300 °C. UV-$vis_{(CH_3CN)}$: 500 nm (ε=125000); Φ_{fluo} (518 nm): 0.72; ^{1}H NMR (CD_3OD) δ 1.47 (s, 6H, 2×CH_3), 2.57 (s, 6H, 2×CH_3), 3.80 (t, 2H, J = 6 Hz), 4.09 (t, 2H, J = 6 Hz), 6.00 (s, 2H), 7.02 (d, 1H, J = 8 Hz), 7.13 (t, 1H, J = 3 Hz), 7.18 (d, 1H, J = 3 Hz), 7.46 (t, 1H, J = 8 Hz).

The **19a** (146 mg, 0.38 mmol), I_2 (193 mg, 0.76 mmol) and HIO_3 (133.6 mg, 0.76 mmol) were reacted as described for compound **14**. The crude product was purified by column chromatography (SiO_2 35 g, CH_2Cl_2-MeOH, 97:2) affording 110 mg (0.173 mmol; yield: 45.5%) of **19** as red needles, mp > 300 °C; EA: calcd for $C_{21}H_{21}BF_2I_2N_2O_2$ C, 39.66; H, 3.33; N, 4.40; found: C, 39.88; H, 3.32; N, 4.43; UV-$vis_{(CH_3CN)}$: 531 nm (ε=66000); Φ_{fluo} (559 nm): 0.01; ^{1}H NMR (CD_3OD) δ 1.49 (s, 6H, 2×CH_3), 2.67 (s, 6H, 2×CH_3), 3.82 (t, 2H, J = 6 Hz), 4.10 (t, 2H, J = 6 Hz), 7.06 (d, 1H, J = 12 Hz), 7.14 (m, 2H), 7.52 (td, 1H, J_1 = 9 Hz, J_2 = 3 Hz); ^{13}C NMR ($CDCl_3$) δ 16.04, 16.36, 61.03, 70.31, 85.39, 112.82, 122.34, 123.83, 129.60, 131.36, 138.52, 144.80, 155.52, 156.56; MS (ESI): M^+ found: 635.97 calcd for $C_{21}H_{21}BF_2I_2N_2O_2$ 636.02; HPLC: retention time = 9'42'' (98.5%); Photo-degradation t_{60}: 53%, t_{120}: 66%.

4,4-difluoro-2,6-diiodo-1,3,5,7-tetramethyl-8-[4'-(4''-chlorobuthoxy)phenyl)]-4-bora-3a,4adiaza-s-indacene (20). 2,4-Dimethylpyrrole (340 µL, 3.30 mmol) and 4-(4-chlorobuthoxy)benzaldehyde (319 mg, 1.50 mmol) were reacted as described for compound **14a**.

The raw material was purified by column chromatography (SiO_2 55 g, CH_2Cl_2) affording 149 mg (0.345 mmol; yield: 23.0%) of **20a** as an orange needles. mp > 300 °C. UV-vis$_{(CH_3CN)}$: 502 nm (ε=118000); Φ_{fluo} (520 nm): 0.79; ^{1}H NMR (CD_3OD) δ 1.45 (s, 6H, 2×CH_3), 2.03 (m, 4H, 2×CH_2), 2.57 (s, 6H, 2×CH_3), 3.67 (t, 2H, J = 7 Hz), 4.08 (t, 2H, J = 7 Hz), 6.00 (s, 2H), 7.02 (d, 2H, J = 10 Hz), 7.18 (t, 2H, J = 10 Hz).

The **20a** (138 mg, 0.32 mmol), I_2 (162.4 mg, 0.64 mmol) and HIO_3 (112.6 mg, 0.64 mmol) were reacted as described for compound **14**. The crude product was purified by column chromatography (SiO_2 35 g, CH_2Cl_2) affording 98 mg (0.143 mmol; yield: 44.7%) of **20** as red needles, mp > 300 °C; EA: calcd for $C_{23}H_{24}BClF_2I_2N_2O$ C, 40.47; H, 3.54; N, 4.10; found: C, 40.21; H, 3.52; N, 4.11; UV-vis$_{(CH_3CN)}$: 528 nm (ε=52000); Φ_{fluo} (549 nm): 0.04; ^{1}H NMR (CD_3OD) δ 1.51 (s, 6H, 2×CH_3), 2.05 (m, 4H, 2xCH_2), 2.66 (s, 6H, 2×CH_3), 3.68 (t, 2H, J = 8 Hz), 4.10 (t, 2H, J = 8 Hz), 7.04 (d, 2H, J = 11 Hz), 7.15 (d, 2H, J = 11 Hz); ^{13}C NMR ($CDCl_3$) δ 16.00, 17.18, 26.63, 29.31, 44.61, 67.24, 85.53, 115.36, 126.79, 129.15, 131.74, 141.76, 145.35, 156.61, 159.86;MS (ESI): M^+ found: 682.30 calcd for $C_{23}H_{24}BClF_2I_2N_2O$ 682.52; HPLC: retention time = 17'19'' (99.1%); Photo-degradation t_{60}: 59%, t_{120}: 75%.

4,4-difluoro-2,6-diiodo-1,3,5,7-tetramethyl-8-(2',6'-dichloro-4'-nitrophenyl)-4-bora-3a,4adiaza-s-indacene (21). 2,4-Dimethylpyrrole (340 µL, 3.30 mmol) and 2,6-dichloro-4-nitrobenzaldehyde (220 mg, 1.50 mmol) were reacted as described for compound **14a**. The raw material was purified by column chromatography (SiO_2 55 g, petroleum ether-CH_2Cl_2, 1:1) affording 100 mg (0.228 mmol; yield: 15.2%) of **21a** as an orange needles. mp > 300 °C. UV-vis$_{(CH_3CN)}$: 504 nm (ε=112000); Φ_{fluo} (522 nm): 0.77; ^{1}H NMR ($CDCl_3$) δ 1.52 (s, 6H, 2×CH_3), 2.65 (s, 6H, 2×CH_3), 6.02 (s, 2H), 8.38 (s, 2H).

The **21a** (87.6 mg, 0.20 mmol), I_2 (101.5 mg, 0.40 mmol) and HIO_3 (70.4 mg, 0.40 mmol) were reacted as described for compound **14**. The crude product was purified by column chromatography (SiO_2 30 g, petroleum ether-CH_2Cl_2, 6:4) affording 82 mg (0.119 mmol; yield: 59.5%) of **21** as red needles, mp > 300 °C; EA: calcd for $C_{19}H_{14}BCl_2F_2I_2N_3O_2$ C, 33.08; H, 2.05; N, 6.09; found: C,

33.11; H, 2.05; N, 6.07; UV-vis$_{(CH_3CN)}$: 530 nm (ε=56000); Φ_{fluo} (547 nm): 0.02; ^{1}H NMR ($CDCl_3$) δ 1.52 (s, 6H, 2×CH_3), 2.70 (s, 6H, 2×CH_3), 8.38 (s, 2H); ^{13}C NMR ($CDCl_3$) δ 15.87, 16.43, 85.18, 123.38, 130.58, 135.37, 138.45, 140.32, 144.63, 149.09, 158.13; MS (ESI): M^+ found: 689.68 calcd for $C_{19}H_{14}BCl_2F_2I_2N_3O_2$ 689.86; HPLC: retention time = 10'57'' (99.8%); Photo-degradation t_{60}: 57%, t_{120}: 71%.

4,4-difluoro-2,6-diiodo-1,3,5,7-tetramethyl-8-(2',4',6'-trimethoxyphenyl)-4-bora-3a,4adiaza-s-indacene (22). 2,4-Dimethylpyrrole (340 µL, 3.30 mmol) and 2,4,6-trimethoxybenzaldehyde (294.3 mg, 1.50 mmol) were reacted as described for compound **14a**. The raw material was purified by column chromatography (SiO_2 55 g, petroleum CH_2Cl_2-MeOH, 99:1) affording 148 mg (0.357 mmol; yield: 23.8%) of **22a** as an orange needles. mp > 300 °C. UV-vis$_{(CH_3CN)}$: 502 nm (ε=113000); Φ_{fluo} (521 nm): 0.65; ^{1}H NMR ($CDCl_3$) δ 1.57 (s, 6H, 2×CH_3), 2.62 (s, 6H, 2×CH_3), 3.72 (s, 6H, 2×OCH_3), 3.91 (s, 3H, OCH_3), 6.00 (s, 2H), 6.26 (s, 2H).

The **22a** (141 mg, 0.34 mmol), I_2 (170 mg, 0.67 mmol) and HIO_3 (118 mg, 0.67 mmol) were reacted as described for compound **14**. The crude product was purified by column chromatography (SiO_2 30 g, CH_2Cl_2-MeOH, 99:1) affording 121 mg (0.182 mmol; yield: 53.5%) of **22** as red needles, mp > 300 °C; EA: calcd for $C_{22}H_{23}BF_2I_2N_2O_3$ C, 39.67; H, 3.48; N, 4.21; found: C, 39.70; H, 3.47; N, 4.23; UV-vis$_{(CH_3CN)}$: 530 nm (ε=45000); Φ_{fluo} (554 nm): 0.01; ^{1}H NMR ($CDCl_3$) δ 1.57 (s, 6H, 2×CH_3), 2.65 (s, 6H, 2×CH_3), 3.72 (s, 6H, 2×OCH_3), 3.91 (s, 3H, OCH_3), 6.24 (s, 2H); ^{13}C NMR ($CDCl_3$) δ 16.10, 17.01, 55.03, 57.65, 84.99, 108.58, 124.34, 131.97, 137.45, 145.09, 156.13, 156.45, 156.89; MS (ESI): M^+ found: 665.96 calcd for $C_{22}H_{23}BF_2I_2N_2O_3$ 666.05; HPLC: retention time = 10'52'' (95.6%); Photo-degradation t_{60}: 55%, t_{120}: 74%.

4,4-difluoro-2,6-diiodo-1,3,5,7-tetramethyl-8-(4'-cyanophenyl)-4-bora-3a,4adiaza-s-indacene (23). 2,4-Dimethylpyrrole (340 µL, 3.30 mmol) and 4-cyanobenzaldehyde (197 mg, 1.50 mmol) were reacted as described for compound **14a**. The raw material was purified by column chromatography (SiO_2 50 g, CH_2Cl_2) affording 169 mg (0.484 mmol; yield: 32.3%) of **23a** as an

orange needles. mp > 300 °C. UV-vis$_{(CH_3CN)}$: 498 nm (ε=111000); Φ_{fluo} (516 nm): 0.81; ^{1}H NMR ($CDCl_3$) δ 1.37 (s, 6H, 2×CH_3), 2.67 (s, 6H, 2×CH_3), 6.02 (s, 2H), 7.47 (d, 2H, J = 10 Hz), 7.88 (d, 2H, J = 10 Hz).

The **23a** (148 mg, 0.44 mmol), I_2 (223.3 mg, 0.88 mmol) and HIO_3 (155 mg, 0.88 mmol) were reacted as described for compound **14**. The crude product was purified by column chromatography (SiO_2 40 g, CH_2Cl_2) affording 189 mg (0.314 mmol; yield: 71.4%) of **23** as red needles, mp > 300 °C; EA: calcd for $C_{20}H_{16}BF_2I_2N_3$ C, 39.97; H, 2.68; N, 6.99; found: C, 40.01; H, 2.70; N, 7.02; UV-vis$_{(CH_3CN)}$: 530 nm (ε=76000); Φ_{fluo} (553 nm): 0.03; ^{1}H NMR ($CDCl_3$) δ 1.39 (s, 6H, 2×CH_3), 2.68 (s, 6H, 2×CH_3), 7.47 (d, 2H, J = 10 Hz), 7.87 (d, 2H, J = 10 Hz); ^{13}C NMR ($CDCl_3$) δ 16.14, 17.25, 86.35, 113.91, 117.84, 129.23, 130.61, 133.16, 138.15, 139.73, 144.78, 157.98; MS (ESI): M^+ found: 601.00 calcd for $C_{20}H_{16}BF_2I_2N_3$ 600.98; HPLC: retention time = 9'53'' (96.9%); Photo-degradation t_{60}: 53%, t_{120}: 70%.

4,4-difluoro-2,6-diiodo-1,3,5,7-tetramethyl-8-(3',5'-dimethoxyphenyl)-4-bora-3a,4adiaza-s-indacene (24). 2,4-Dimethylpyrrole (340 µL, 3.30 mmol) and 3,5-dimethoxybenzaldehyde (249 mg, 1.50 mmol) were reacted as described for compound **14a**. The raw material was purified by column chromatography (SiO_2 50 g, CH_2Cl_2-MeOH, 99:1) affording 189 mg (0.492 mmol; yield: 32.8%) of **24a** as an orange needles. mp > 300 °C. UV-vis$_{(CH_3CN)}$: 498 nm (ε=111000); Φ_{fluo} (517 nm): 0.74; ^{1}H NMR (CD_3OD) δ 1.55 (s, 6H, 2×CH_3), 2.63 (s, 6H, 2×CH_3), 3.80 (s, 6H, 2×OCH_3), 6.01 (s, 2H), 6.42 (d, 2H, J = 2.5 Hz), 6.60 (d, 1H, J = 2.5 Hz).

The **24a** (181 mg, 0.47 mmol), I_2 (238.6 mg, 0.94 mmol) and HIO_3 (165.3 mg, 0.94 mmol) were reacted as described for compound **14**. The crude product was purified by column chromatography (SiO_2 40 g, CH_2Cl_2) affording 223 mg (0.351 mmol; yield: 74.7%) of **24** as red needles, mp > 300 °C; EA: calcd for $C_{21}H_{21}BF_2I_2N_2O_2$ C, 39.66; H, 3.33; N, 4.40; found: C, 39.71; H, 3.33; N, 4.39; UV-vis$_{(CH_3CN)}$: 533 nm (ε=46000); Φ_{fluo} (556 nm): 0.02; ^{1}H NMR ($CDCl_3$) δ 1.58 (s, 6H, 2×CH_3), 2.66 (s, 6H, 2×CH_3), 3.82 (s, 6H, 2×OCH_3), 6.43 (d, 2H, J = 2.5 Hz), 6.60 (d, 1H, J = 2.5 Hz); ^{13}C

NMR ($CDCl_3$) δ 16.26, 17.03, 57.02, 85.39, 109.08, 112.87, 122.99, 131.89, 139.22, 144.76, 156.03, 157.20; MS (ESI): M^+ found: 636.09 calcd for $C_{21}H_{21}BF_2I_2N_2O_2$ 636.02; HPLC: retention time = 12'37'' (99.0%); Photo-degradation t_{60}: 56%, t_{120}: 68%.

Fluorescence properties and Quantum Yield of Fluorescence.

Steady-state fluorescence spectroscopic studies were performed with a Jasco FP-750 spectrofluorimeter. The slit width was 2.5 nm for both excitation and emission. Values of absorbance, necessary for the equation described below, were obtained on a Varian Cary 50 Scan instrument by using the same solutions of the fluorescence measurements. The relative quantum efficiencies of fluorescence of each BODIPY derivative was obtained comparing the emission spectra of the test sample, prepared as dichloromethane solution (dieletric constants 9.14), with that of a 0.1 M NaOH solution of fluorescein excited at 490 nm, whose quantum efficiency literature value is 0.85 [20]. The quantum efficiencies of fluorescence (Φ_{fluo}) of the BODIPYs were calculated according to the following equation (I_{fluo} is the fluorescence intensity at the specific excitation wavelength, Abs denotes the absorbance at the excitation wavelength):

$$\Phi_{fluo}^{sample}=\Phi_{fluo}^{standard}\times(I_{fluo}^{sample}/I_{fluo}^{standard})\times(Abs^{standard}/Abs^{sample})$$

Comparative Singlet-Oxygen generation measurements.

A solution of aerated isopropanol containing 50 μM of 1,3-diphenylisobenzofuran (DPBF) and 2.5 μM of photosensitizers was prepared in a glass flask and kept in the dark; 2 mL of this solution were transferred into a cuvette, placed in the UV-vis instrument and irradiated from the open top side with the green LED source, at room temperature and for the time required to observe the chemical event (maximum 20 min.). The DPBF absorbance decrease was measured at 410 nm at fixed time intervals, as defined for each experiment. Two controls were also set up, the first to study the effect of the light irradiating a DPBF-isopropanol solution in the absence of photosensitizer (negative control) and the second irradiating a DPBF-isopropanol and Rose Bengal (2.5 μM) (comparative normalizing data). The rate of singlet oxygen production for each PS was obtained plotting the variation of DPBF absorbance over the irradiation time and the relative singlet oxygen

generation rates were normalized with respect to the rate determined by using Rose Bengal as standard [21].

Photo-degradation of the BODIPYs.

Phosphate Buffer Solution (PBS) of each PS (10 μM) was prepared in a flask. These solutions were irradiated, for 2 h at room temperature, with the green LED; within this period 1 mL sample was collected after 60 min and at 120 min and analysed with the spectrophotometer. The percentage of photo-degradation was determined at 60 (t_{60}) and 120 (t_{120}) min as the ratio of the absorption intensity with respect to absorption measured at t_0.

Cytotoxicity studies.

The human ovarian carcinoma cell line SKOV3 was obtained from the American Type Culture Collection (Rockville, MD, USA) and maintained in Dulbecco's modified Eagle medium-F12 (DMEM-F12, Mascia-Brunelli, Milano, Italy) supplemented with 10% fetal bovine serum, 1% glutamine and 0.5% antibiotic mixture (penicillin, streptomycin and neomycin), in standard culture conditions at 37 °C in a humidified 5% CO_2 atmosphere.

The antiproliferative effect of each BODIPY was assessed using the MTT assay [22]. Briefly, 1.5×10^3 cells/well were seeded onto 96-wells plate and allowed to grow for 48 h prior to the treatment with 100 μL of BODIPY solutions at different concentration. These solutions were prepared by dilution with PBS of a stock BODIPY solution, prepared in acetone or DMSO at 1 mM concentration, according to the PS solubility.

The dilution of the stock BODIPY solutions were made in order to get a cell non toxic concentration of the organic solvent in the solution used in the cells treatment (below 1%).

After 24 h, the BODIPY-containing medium was replaced by fresh PBS, and cells were irradiated under visible light for 2 h using a green LED (fluence 25.2 J/cm^2). At the end of irradiation, cells were incubated in the dark for 24 h at 37 °C in drug-free medium then MTT was added to each well (final concentration 0.4 mg/mL) and left reacting for 3 h at 37 °C. The formazan crystals, formed

through MTT metabolism by viable cells, were dissolved in DMSO and the optical densities were measured at 570 nm using a Universal Microplate Reader EL800 (Bio-Tek Instruments).

Possible intrinsic cytotoxic effects (i.e. not photo induced cell death) of the BODIPYs were assessed on control cultures kept in the dark and treated, as described above, with concentrations of BODIPY tenfold higher than those used in the PDT assays.

IC_{50} values (*i.e.* the concentration affecting 50% of cell survival fraction) were obtained by nonlinear regression analysis, using the GraphPad PRISM 3.03 software (GraphPad Software Inc., San Diego CA).

Intra-Cellular localization.

Non-iodinated BODIPYs, namely those featuring a hydrogen atom on the 2,6 positions (H_2-BODIPY), were used in these experiments because of these molecules are characterized by high fluorescence, a useful property for the detection of the PS inside the cells. Thus, SKOV3 cells were seeded onto coverslips (10000 cells), allowed to grow for 48 h and subsequently treated with the desired H_2-BODIPY at a concentration ten time higher than the IC_{50} values, as determined in the MTT assays with the iodinated derivatives. After 24 h, cell attached to coverslips were washed three time in 1X PBS and fixed in 3% paraformaldehyde for at least 10 min and then washed in 1X PBS three times. Coverslips were mounted on microscope slides. Images were acquired using a LEICA TCS SP8 X confocal laser scanning microscope.

Flow cytometric studies.

The effects of compound **2** were assessed at different concentrations (0.5, 1 and 2 nM) on SKOV3 cell line. Following the described treatment (24 h exposure to the drugs, 2 h irradiation in drug-free PBS and 24 incubation in drug-free medium) the percentage of apoptotic cells and cell cycle distribution were assessed using Propidium Iodide (PI) staining. Cells were fixed in 0.5 mL of ice-cold 70% ethanol and stored at −20 °C. Cells were then centrifuged, washed with PBS, resuspended in the dying solution (50 μg/mL propidium iodide, 20 μg/mL RNase in 1× PBS) and analyzed. The

percentage of apoptotic cells in each sample was determined based on the sub-G1 peaks detected in monoparametric histograms.

Intracellular ROS levels at the end of compound **2** treatment was assessed using 2,7-Dichlorodihydrofluorescein diacetate (DCHF-DA) as a fluorogenic probe. DCHF-DA is cleaved by intracellular esterases to release the corresponding dichlorodihydrofluorescein derivative (non-fluorescent), which is readily oxidized to dichlorofluorescein (DCF) by reactive oxygen species (ROS).

Cells were treated with compound **2** at 0.5, 1 and 2 nM for 24 h, followed by 2 h irradiation. Cells were then detached, washed and resuspended in PBS containing 10 μM DCFH-DA and analyzed. after 45 min dark incubation at 37 °C.

All samples were analyzed with FACScalibur flow cytometer (Becton–Dickinson, Mountain View, CA, USA) equipped with a 15 mW, 488 nm air cooled Argon ion laser. Fluorescent emissions were collected through a 530 nm band-pass filter for fluorescein, a 575 nm bandpass filter for PI. At least 10,000 events were analyzed for each sample. Data were processed using CellQuest software (Becton-Dickinson).

QSAR Analysis: experimental procedures.

In order to perform Quantitative Structure Activity Relationship (QSAR) analysis, the IC_{50} concentrations for the 24 molecules were expressed in logarithmical form, log (IC_{50}). The three-dimensional structures of the studied BODIPYs were designed in the computational software HYPERCHEM [23] and their conformation was optimized at the minimum energy by the semi-empirical Austin Model 1 (AM1) method. The topological, geometrical and chemical diversity of compounds was numerically encoded by theoretical molecular descriptors calculated by DRAGON (ver. 5) software [24] using the atomic coordinates (x, y, z) of the minimum energy conformation of the three dimensional structures as input. More than 1200 mono-, bi- and three-dimensional molecular descriptors were calculated. Moreover, some quantum chemicals descriptors such as HOMO, LUMO, HOMO-LUMO Gap (DHL), Ionization Potential, Binding Energy (calculated by

semi-empirical AM1 method in HYPERCHEM), and experimental properties such as HPLC retention time (Rt) and $^1O_2$ production rates ($^1O_2$) were added as potential modeling variables for the descriptors selection during the model development. Then variables were analyzed in a pre-reduction phase where constant (for more than the 80%) and pairwise correlated descriptors (one variables was deleted when there was more than 98% pairwise correlation,) were excluded to delete null and redundant information. The final reduced set of 427 molecular descriptors was used as input for explorative chemometric analyses and QSAR models development. The Genetic Algorithm variable subset selection (GA-VSS) and Multiple Linear Regression (MLR) by the Ordinary Least Square (OLS) were performed by the QSARINS (QSAR-INSubria) software [25,26]. All the possible combination of two descriptors were investigated by the all-subset procedure. Then, the GA was applied (3000 iterations) to find the best three variable combinations starting from a population of 100 models; Q^2_{loo} (leave one out) was used as fitness function to be optimized during the variable selection procedure. The robustness and stability of the models were evaluated by Q^2_{loo}, Q^2_{lmo} (leave more out) and CCC (concordance correlation coefficient) [27] in cross validation. To guarantee good internally predictive models, the values of the Q^2 functions should be around 0.7 and the CCC values should be around 0.85 [28]. Cross Validation is an iterative process that involves a sequential splitting of the original training set in different test sets on which the fitting is re-tested. In particular, Q^2_{loo} and Q^2_{lmo} measure the internal predictive capacity when, respectively, one or more compounds, in a series of iterations, are excluded from the computation and then predicted by the model recalculated on the remaining objects. For the leave more out procedure we run 2000 iterations with the 30% of compounds excluded from computation for each iteration. Moreover, also permutation testing, by *y*-scrambling procedure, was performed to exclude by chance models. The test is performed calculating, in a series of iterations, the quality of the model (usually R^2), randomly modifying the sequence of the response vector *y*, by assigning to each object a response randomly selected from the true responses. Low values of the averaged R^2 scrambled (R^2_{ys}) are indicative of a well founded (not by chance) original model [29,30]. A further

measure to define the accuracy of the proposed QSAR model is also the RMSE (Root Mean Square Error) that summarizes the overall error of the model. It is calculated as the root square of the sum of the squared errors in predictions divided by their total number ($RMSE_{tr}$ and $RMSE_{cv}$, calculated separately for the training and the cross validation). Finally, QSAR models must always be verified for their applicability with regard to chemical domain. For this reason we investigated, by Williams plot [29], the presence of outliers (molecules with cross-validated standardized residuals greater than 2.5 deviation unit) and molecules structurally influent in the selection of modelling descriptors and parameters (compounds with leverage value (h) higher than h* (3 p'/n).

Results and Discussion

A series of BODIPYs was synthesized, based on the assumption that the presence of different substituents on an aromatic ring on the *meso* (8) position, would affect both the hydrophobic/hydrophilic balance and the rate of singlet oxygen production of these PSs. The first chemical property is crucial as it can influence the cell penetration and the target of the subcellular localization, both depending on the lipophilicity degree of the photosensitizer [19]. As far as it concerns another fundamental aspect influencing the PDT outcome, i.e. the singlet oxygen generation rate, we have already reported that an aromatic moiety on the BODIPY *meso* position induces different rates depending on the nature of the substituent tethered on the phenyl ring [19].

Chemistry.

The BODIPY derivatives were synthesized *via* acid catalysed condensation of the desired aromatic aldehyde (11 different aldehydes were used) with 2,4-dimethylpyrrole in the presence of catalytic amount of trifluoroacetic acid (TFA), following the general methods described by Akkaya and Liu [31,32]. Either dichloromethane (DCM) or tetrahydrofuran (THF) were used as solvent in the BODIPY syntheses, depending on the solubility of the aldehyde; in particular, THF was conveniently used when hydroxy substituted aldehydes were the reactant. The disappearance of the aldehyde spot in the TLC analysis, fulfilled for the reaction control, indicates the formation of dipyrrolylmethane that was subsequently dehydrogenated to dipyrrolylmethene with 2,3-dichloro-

5,6-dicyano-1,4-benzoquinone (DDQ) added in the same flask. In the end, the mixture was treated with $BF_3{\cdot}Et_2O$ and Et_3N thus achieving the complete synthesis of the desired BODIPYs. Each compound has been isolated as pure solid after a single chromatographic step of purification (Scheme 1).

The 2,6-positions of each BODIPY were modified with the insertion of iodine atoms (Scheme 1) to favour the passage of the PS from the singlet to the triplet excited state following irradiation, thus increasing the singlet oxygen production rate. Regarding the iodination process, we found that the conditions reported in the literature (I_2, HIO_3, 60 °C, 20 min) [14] cause a partial degradation of the dipyrrolylmethene skeleton, leading to extremely low yields in the desired iodinated boron-compounds. The successful recovery of the iodinated derivatives in good yields (> 45%) was obtained using a lower temperature (20–25 °C) and increasing the reaction time to 15–18 h.

Scheme 1

The BODIPYs synthesized in this work and those already reported [19] are listed in Figure 1. Each compound was completely characterized in terms of UV-vis absorption spectra, quantum yield of fluorescence, NMR and MS spectra. In addition, for a better understanding of the photodynamic process, HPLC retention time (Rt) and singlet oxygen generation were also measured.

Figure 1

The lipophilicity of organic compounds is generally measured by considering the partition coefficients (P) in a 1-octanol /water mixture. The P values are commonly obtained following Uv-vis analysis of both the organic and the aqueous phase according to the equation Log P = Log $[PS]_{octanol}/[PS]_{water}$ This method cannot be applied for those compounds that hardly distribute in both the phases (being or highly lipophilic or, *vice versa*, extremely hydrophilic). When the method based on absorbance (or the more sensible fluorescence) cannot be applied, as for our molecules, a comparative degree of lipophilicity of chemicals can be determined evaluating the HPLC retention time (Rt) on a RP-C18 column, in the event that the molecules belong to a homogeneous series and performing the analyses under standardized conditions.

In the case of the described BODIPYs, we can assert that the aromatic group in *meso* position modifies the hydrophilicity of these molecules (table 1). Considering the retention time values, these BODIPYs could be arbitrarily divided in three groups: the first group, characterized by Rt values below 10 min, includes the hydrophilic BODIPYs (**8**, **14**, **16**, **17**, **19**, **21** and **23**) among which the most polar is BODIPY **8**, characterized by the presence of two chlorine atom in the *ortho*, *ortho'* position of the phenyl ring. With the only exception of BODIPY **19,** characterized by the presence of a ethoxy-alcohol appendix, the molecules belonging to the hydrophilic set are characterized by the presence of electron withdrawing substituent such as chloride atoms, cyano and nitro groups. A second group of compounds can be envisaged considering the Rt interval between 10 and 15 min. This is the most numerous set as eleven molecules (**2**, **3**, **4**, **5**, **9**, **11**, **12**, **13**, **15**, **22** and **24**) show an intermediate level of the hydrophilic/lipophilic ratio. The presence of heterogeneous substituents on the aromatic ring characterizes the structure of these BODIPYs. In fact, the aromatic ring of the second group show the presence of either electron-withdrawing or -donating group. Many phenyls show the presence of one or more methoxy groups (one in compounds **2**, **3** and **15**; two in compound **24** and three in **22**). Two molecules show one phenolic group that should ensure a high hydrophilicity. They are expected with shorter Rt then to be part of the first set of polar molecules rather than the second set. However, the presence of large iodine atom(s) nearby the OH masks the hydrophilic effect of the OH (compounds **4** and **5**). Two BODIPYs, belonging to this second set of polarity, are characterized by the presence of pyridyl moiety (compound **11** and **12**) that could be protonated in acidic aqueous medium. At pH 7.2 (the buffered aqueous phase used in these HPLC analyses), the pyridyl group is present as free base thus showing a weak interaction with the lipophilic stationary phase of the C18 columns. The pentafluorophenyl substituted compound **9** fall in this group of molecules because of the two opposite effects of the fluorine atoms. Their electronegativity increases the polarity of the BODIPY but, it is also known, the high hydrophobicity of polyfluorinated compounds. The observed Rt is the result of a balance of these two effect. Quite surprisingly, compound **13**, the only one characterized by the presence of a hydrogen atom on the

meso position, belongs to the medium polarity set of BODIPYs. The last group of BODIPYs (Rt > 15 min,) includes the most lipophilic compounds (**1**, **6**, **7**, **10**, **18** and **20**) i.e. those characterized by the highest affinity for the stationary phase. More precisely, the molecules featuring the nonpolar naphthyl group (**6**, **7**) show a greater affinity for the C18 reversed phase HPLC column, as witnessed by the highest Rt. A similar strong interaction between the BODIPYs and the stationary phase was also observed for compounds **10** and **20**, both characterized by the presence of a long, nonpolar appendix. As far it concerns the presence of large halogens (Br and I), as in compounds **1** and **18**, it can be assumed that the presence of these atoms increases the lipophilicity of the molecules. It is worth noting the striking difference of polarity between the compounds bearing Br and I with respect to the chlorine substituted BODIPY (**8**).

The fluorescence data, reported in Table 1, have been normalized with respect to the value obtained using fluorescein as standard [20]. As expected, the data show a very low value of fluorescence quantum yield as the iodine atoms exert the well known ISC effect, thus shifting the singlet excited state into a lower energetic triplet state. This event prompts a nearly complete inhibition of fluorescence to the advantage of a very high rate of singlet oxygen generation.

The production of $^1O_2$ for each photosensitizer was indirectly determined measuring the disappearance of the absorption band (at 410 nm) of the 1,3-diphenylisobenzofuran (DPBF), a well-known $^1O_2$ scavenger. The experiments were carried out following a literature method, using isopropanol as solvent with a 50 μM initial concentration of DPBF and in the presence of 2.5 μM of BODIPY. Irradiation was carried out with a green LED device. The choice of green light ensures a high level of electronic excitation of these PSs because of the good overlap between the λ_{max} of absorbance of BODIPYs and the emission wavelength of the green LED, as well as with the absorbance profile of the standard dye.

The relative rates of singlet oxygen ($^1O_2$) production were obtained comparing the kinetic of DPBF degradation obtained with the BODIPY and with a reference molecule. In this work Rose Bengal, widely recognized as a high singlet oxygen producer, was used as standard [21].

The relative rates reported in Tables 1 show that all the tested BODIPYs are characterized by intense singlet oxygen production with rates comparable or higher than Rose Bengal. Eleven compounds showed a very high rate of $^1O_2$ production and, among them, compounds **11**, **15**, **16** and **17** produce $^1O_2$ twice as much with respect to the reference compound.

Table 1

In *in vivo* PDT applications, the photo-degradation of the photosensitizer plays an important role. Indeed, any PS with a high stability can turn out to be highly phototoxic for a prolonged time after the treatment. For this reason, we have evaluated the stability of the BODIPYs irradiating an aqueous 10 μM solution with the green LED then recording the absorbance at 60 and 120 min. The results show that the photo-degradation of BODIPYs has an average value of 55% after 60 min whereas it is approximately 70% after 120 min. It is evident that the degradation process rapidly occurs at high concentrations, whereas it slows down when the majority of the PS has already decomposed, to confirm the result previously reported by us [19]. According to the literature, it seems that the extension of the degradation of BODIPYs under green light irradiation strongly depends on the molecular structure [17].

Cytotoxicity Assays.

The IC_{50} values from dose/response curves obtained in SKOV3 cells following exposure to the different PSs for 24 h and irradiation with Green LED device for 2 h (fluence 25.2 J/cm^2) are reported in Table 1. The intrinsic cytotoxicity of PSs was assessed omitting the irradiation step in the treatment protocol observing a negligible effect in all cases, although PS concentrations 10-fold higher than those used for PDT experiments were considered.

All the *meso* aryl substituted compounds showed a very high *in vitro* phototoxicity with IC_{50} value in the range 0.65 – 8.03 nM. The comparison of the activity of compound **13** (IC_{50} = 28.75 nM), characterized by the presence of a hydrogen atom in position 8, with those of all the other BODIPYs clearly indicates that the presence of an aromatic ring (independently from the presence of whatever substituents on it) on the *meso* position of the BODIPY frame is fundamental to ensure a high cell-

killing efficacy. Even the less active "*meso*" aryl substituted BODIPYs, compounds **10** and **14**, show a remarkable higher efficacy as their IC_{50} values are 8.03 and 7.77 nM, respectively.

Besides the striking evidence of the negative effect exerted by the absence of substituent on the *meso* BODIPY position, the tumor cell-killing efficacy of the aryl substituted BODIPYs does not give a clear indication about which kind of substituent can ensure an activating effect or which has a clear inhibiting effect. The two less active compounds (**10** and **14**) are characterized by the presence of electron withdrawing and/or bulky substituents on the phenyl and are among the most polar. In this context, the presence of a nitro group seems to decrease the efficacy of the photodynamic action as evidenced by the low activity of compound **21** (2,6-dichloro-4-nitrophenyl; IC_{50} = 3.93 nM) and of compound **14** (2-chloro-6-nitrophenyl; IC_{50} = 7.77 nM) as compared with the second best BODIPY **8** (2,6-dichlorophenyl; IC_{50} = 0.77 nM). However, the effect of the presence of a nitro group is not so clear as compound **16** (4-nitrophenyl) has shown a good activity (IC_{50} = 2.01 nM).

It seems that the electronic properties, position(s) or steric hindrance of the substituents, present on the *meso* aromatic ring, do not allow to point out a specific rule to predict the cytotoxicity of these photosensitizers. Actually, considering the two more active compounds, BODIPY **2** and **8** (IC_{50} = 0.65 and 0.77 nM respectively) are characterized by groups located in different positions and with different electronic effects (*p*-OMe and *o,o*'-chlorine atoms as appendix, respectively).

Thus we made the effort to correlate the cell-killing efficacy (IC_{50} Values) with two chemico-physical properties (HPLC Rt and $^1O_2$ production rates) reported for these compounds with the only exclusion of compound **13** because of its striking different efficacy in the photo-induced cell-killing.

In figure 2 the IC_{50} values were correlated with the singlet oxygen generation (A) and with the lipophilicity degree (B). For the correlation, we normalize the data to respect the maximum value of each series.

Unfortunately we could not observe any correlation, in fact the R^2 = 0.0064 for IC_{50} versus $^1O_2$ and R^2 = 0.0111 for IC_{50} versus Rt were found, respectively, then it is impossible understand the activity of these molecules based on lipophilicity or singlet oxygen production.

Figure 2

Someway better results should be obtained with a more sophisticated QSAR analyses comparing the results of photoinduced cell-killing activity with many different structure parameters.

QSAR analysis.

Quantitative Structure Activity Relationship (QSAR) modelling, based on theoretical molecular descriptors, was performed in order to verify which structural features are correlated to phototoxicity of BODIPYs against a tumor cell line.

The log (IC_{50}) values for the 24 BODIPYs were used as responses (y), while mono-, bi- and three-dimensional theoretical molecular descriptors were used as predictive variables (x) in the development of descriptive MLR QSAR models in a specified structural Applicability Domain. As described in the Experimental section, we applied an evolutionary variable selection procedure, called Genetic Algorithm (GA-VSS), to find the best combination of descriptors able to justify the photodynamic cytotoxicity among the whole molecular descriptors dataset. This is done because we cannot know, *a priori*, which descriptors could be related with the activity of the BODIPY describing significant structural features. Statistical internal validation was performed to assess the stability of the models when subjected to perturbation and to ensure a certain degree of generality, independently from the training set used for their development. Validation parameters (Q^2_{loo}, Q^2_{lmo}, CCC_{cv}) were used as criteria for the model selection in the GA population. In table 2 the best two models, with similar statistical performances and based on combination of three descriptors with similar structural meaning, are proposed.

Table 2

Both models have high fitting values and good validation parameters indicating that the models have very good descriptive performances and are stable, robust and internally predictive. The RMSE values, expressed in log unit, are low, indicating that the models have an accuracy of at least the 90%, both in fitting and in cross validation.

The plot of predicted and experimental data, the equation of the presented QSAR models and the Williams plot are reported in figure 3.

Figure 3

The most important descriptors able to model the phototoxicity in both models are the GETAWAY descriptors (GEometry, Topology, and Atom-Weights AssemblY) R2e+, R3p+ and R3v+. GETAWAY descriptors derive from the molecular influence matrix (MIM) or from the influence/distance matrix and encode information for structural fragments and structure-properties correlations. In other words, these descriptors are based on the spatial autocorrelation combining 3-D features of the molecules and their physiochemical properties such as atomic mass, polarizability, van der Waals volume, and electronegativity. In particular, R2e+ encodes for the maximal autocorrelation (at topological distance of two bonds) weighted by the atomic Sanderson electronegativity. This descriptor is present in both models, with a positive coefficient meaning that the presence of electronegative substituents is influent in decreasing the phototoxicity.

R3p+ encodes for the maximal autocorrelation (at topological distance of three bonds) weighted by the atomic polarizability and R3v+ calculates the maximum autocorrelation value (at topological distance of three bonds) weighted by atomic van der Waals volume. These two descriptors are selected alternatively in the two proposed models; they have negative coefficients, therefore chemicals with higher values of these descriptors are among the most active.

Overall, these descriptors give information regarding to the influence of electronegativity, polarizability and molecular volume of different molecules within our data set. The other two molecular descriptors, directly correlated with activity, are JIG8 and ARR. The JIG8 encodes for the mean topological charge index and gives information about charge transfer between pairs of atoms and therefore global charge transfer in the molecule. The ARR encodes for the aromatic ratio (number of aromatic bonds over the total number of bonds excluded those with Hydrogen) assuming higher values for compounds with more aromatic rings (such as **6**, **7**, **10**).

The analysis of the chemical applicability domain with the leverage approach (figure 3 b and d) allows us to verify the presence of molecules influential for some peculiarities in their structure or of outliers for the calculated response. In both models BODIPY **13** has *h* values greater than the cutoff *h**, therefore it is a high leverage compound, which has a great influence in selecting model descriptors. It is important to note that **13** is the only one BODIPY of our set without an aryl substituent and characterized by the lowest activity, thus it can be considered as reference compound for the subsequent evaluation of the effect of the *meso* aryl group on the photoinduced toxicity. For this reason **13** has been included in the dataset. Concerning outliers for the response, only compound **15** was predicted with a standardized residual greater than 2.5 in model 2, while it was well predicted by model 1.

In order to verify the contemporaneous influence of all the modelling descriptors in the distribution of the studied chemicals, we performed a Principal Component Analysis (PCA) of the selected molecular descriptors. In figure 4 the biplot of this PCA is reported where BODIPYs (the points) are plotted in the descriptors space (the arrows for the loadings) of the first two principal components (total variance explained 81.15%).

Figure 4

In particular, PC2 (EV% = 39.76) is the principal component more correlated with the response and thus has been plotted in the abscissa axis. Compounds with lowest PC2 values are the less active BODIPYs (left side) while high values of PC2 correspond to more effective molecules (right side). Therefore in the PCA a trend (from left to right) of the photodynamic activity is evident. The least active BODIPY **13** is correctly isolated in left side on the graph.

ARR has in general a positive influence in phototoxicity, highlighting that the photodynamic activity is enhanced by aryl substituents; in fact all the compounds with aromatic rings are located far from **13**. R3v+ and R3p+ are strictly correlated and have a positive influence on the activity trend. The compound **10** is isolated in the upper part of PC1 since it is the biggest with the lowest values of R3v+ and R3p+. On the contrary, R2e+ has a negative correlation with the activity trend.

Thus, less active compounds seem to be mainly characterized by the presence of highly electron withdrawing groups, such as nitro groups (i.e. **14**, **21**). In these compounds, the presence of one or two chlorine atoms, the other substituent present, seem not to contribute to the decrease of the BODIPY efficacy, in fact, the BODIPY **8** is one of the most active compound of the series. It is important to remember that in a multivariate analysis and modelling such as PCA and QSAR the single descriptors are not able to justify independently the end-point; it is only a combination of the selected descriptor set that allows modelling the studied response.

BODIPY cell penetration and percentage of apoptotic cell.

Another possibility to understand the BODIPY's efficacy, is to evaluate the localization of the photosensitizers following cell penetration. To perform this analysis, the non-iodinated derivatives have to be used (H_2-BODIPY) in order to exploit their high quantum yield of fluorescent, assuming that the difference in the structure and chemical weight, between the iodinated and non–iodinated BODIPYs, does not influence the cellular uptake. For all compounds the cellular cultures were treated, over a period of 24 h of incubation, with a concentration of PS ten time higher than those corresponding to the IC_{50} values obtained with the iodinated derivatives. An illustrative example of the result is shown in figure 5. From this analysis become obvious that all BODIPYs were quickly and efficiently internalized by cells and, as already reported for other PSs (porphyrins, chlorins, etc.) [33], they are localized in the cytosol district whereas none fluorescence could be observed in the nucleus.

Figure 5

We also investigated some possible mechanism of action of the most potent BODIPY found in this study (compound **2**). Figure 6 shows that **2** induce a significant increase in the percentage of apoptotic cells, over control samples, at all the tested concentrations. The observed percentage of apoptotic cells never exceed 12%, indicating that cell death induced by compound **2** occurs only in part through apoptosis. A further contribution to the photodynamic effect of compound **2** is evidenced in Figure 7, showing the levels of intracellular oxidizing species in compound **2** treated

SKOV3 cells. Treatment with the BODIPY induce a dose-dependent increase in ROS generation over control levels, even though statistical significance is only achieved when cells were treated with a BODIPY concentration 1.0 nM, which is slightly greater than the IC_{50} value and with a concentration three time higher (2.0 nM).

Cell cycle distribution analysis did not show any difference following treatment with the BODIPY (data not shown).

Figure 6

Figure 7

Conclusions

The panel of iodinated BODIPY here reported has shown a very interesting singlet oxygen production rate, in most cases higher than the one obtained with the reference compound Rose Bengal. In agreement with these data a very promising cell-killing effect following irradiation with a green light emitting LED was observed in *in vitro* assays. The efficacy is undoubtedly correlated to the presence of an aromatic ring on the BODIPY 8 (*meso*) position although none evident indications can be inferred from the presence of electron-withdrawing or electron-donating substituents on the aromatic moiety or according to their position and then their steric hindrance. Actually, the two most active BODIPYs are **2** and **8**, the former characterized by the presence of a methoxy group on the *para* position whereas the latter features two chlorine atoms on the *ortho*, *ortho'* positions. The complete difference in regio-isomerism and in the electronic effects confirming the absence of correlation between the substituents and the efficacy of the photo-induced action. The lipophilic degree also does not influence the PSs efficacies as the compound **2** is among the most lipophilic BODIPYs while compound **8** is part of the hydrophilic set. In conclusion, we have demonstrated the excellent potentiality of BODIPYs as green light activated photosensitizers. Actually the *meso* aryl substituted BODIPYs, also featuring iodine atoms on the pyrrole 2,6 positions, are characterized by high rate of singlet oxygen production and an extensive tumor cells penetration. Consequently, the photo-induced cell-killing efficacy observed in the *in vitro* studies is

exceptionally high as IC_{50} values in the range of 1 – 2 nM concentration are often observed and, in the case of two BODIPYSs, this value is below 1.0 nM. We are aware that the main drawback of this kind of photosensitizers is the wavelength of excitation (green light), that is somewhat far from the optimum-tissue penetrating red region, however it must be considered that early stage and superficial cancers could be successfully treated with these molecules. The next step of this research will be the study of BODIPYs tethered with cationic group to add a polar moiety in these lipophilic structures. The cationic groups can be directly introduced on some of the structure here presented (i.e. exploiting the pyridyl group) or taking advantage of the presence of hydroxyl groups to which a chain of different length, bearing an ammonium ion, can be attached. The presence of a polar moiety should produce a double effect: 1) to facilitate the BODIPYs' solubilization in aqueous medium, thus allowing an easier formulation and, 2) further increases the cancer cells penetration as it is known that amphiphilic molecules, bearing both hydrophobic and hydrophilic moieties, display improved tumor-uptake [33].

References

1. P. Agostinis, K. Berg, K. A. Cengel, T. H. Foster, A. W. Girotti, S. O. Gollnick, S. M. Hahn, M. R. Hamblin, A. Juzeniene, D. Kessel, M. Korbelik, J. Moan, P. Mroz, D. Nowis, J. Piette, B. C. Wilson, J. Golab, Photodynamic therapy of cancer: an update. CA Cancer J. Clin. (2011), 250–281.
2. D. Nowis, M. Makowski, T. Stoklosa, M. Legat, T. Issat, J. Golab, Direct tumor damage mechanisms of photodynamic therapy. Acta Biochim. Pol. 52 (2005) 339–352.
3. R. R. Allison, G. H. Downie, R. Cuenca, X. H. Hu, C. J. Childs, C. H. Sibata, Photosensitizers in clinical PDT. Photodiagnosis Photodyn Ther. 1 (2004) 27-42.
4. J. M. Dabrowski, A. G. Arnaut, Photodynamic therapy (PDT) of cancer: from local to systemic treatment. Photochem and Photobiol Sciences, 14 (2015) 1765-1780.
5. R. K. Pandey, Recent advances in photodynamic therapy, J. Porhyrins Phthalocyanines 4 (2000) 368-373.

6. W. Tronconi, A. Colombo, M. Decesare, R. Marchesini, K. W. Woodburn, J. A. Reiss, D. R. Phillips, F. Zunino, Biodistribution of haematoporphyrin analogues in a lung carcinoma model. Cancer Lett. 88 (1995) 41-48.
7. M. Yee, S. C. Fas, M. Stohlmeyer, T. J. Wandless, K. A. Cimprich, A cell-permeable, activity-based probe for protein and lipid kinases. J. Biol. Chem. 280 (2005) 29053–29059.
8. G. Ulrich, C. Goze, M. Guardigli, A. Roda, R. Ziessel, Pyrromethene dialkynyl borane complexes for "Cascatelle" energy transfer and protein labeling. Angew Chem. Int. Ed. 44 (2005) 3694–3698.
9. S. Y. Moon, N. R. Cha, Y. H. Kim, S. Chang, New Hg^{2+} −selective chromo- and fluoroionophore based upon 8- hydroxyquinoline. J. Org. Chem. 69 (2004) 181–183.
10. T. A. Golovkova, D. V. Kozlov, D. C. Neckers, Synthesis and properties of novel fluorescent switches. J. Org. Chem. 70 (2005) 5545-5549.
11. C. McCusker, J. B. Carroll, V. M. Rotello, Cationic polyhedral oligomeric silsesquioxane (POSS) units as carriers for drug delivery processes. Chem. Commun. (2005) 996-998.
12. T. Yogo, Y. Urano, Y. Ishitsuka, F. Maniwa, T. Nagano, Highly efficient and photostable photosensitizer based on BODIPY chromophore, J. Am. Chem. Soc. 127 (2005) 12162-12163.
13. T. Atilgan, Z. Ekmekci, A. L. Dogan, D. Guc, E. U. Akkaya, Water soluble distyryl-boradiazaindacenes as efficient photosensitizers for photodynamic therapy. Chem Commun. 42 (2006) 4398-4400.
14. S. H. Lim, C. Thivierge, P. Nowak-Sliwinska, J. Han, H. van den Bergh, G. Wagnières, K. Burgess, H. B. Lee, In vitro and in vivo photocytotoxicity of boron dipyrromethene derivatives for photodynamic therapy. Journal Med. Chem. 53 (2010) 2865-2874.
15. J. Karolin, L. B. A. Johansson, L. Strandberg, T. Ny, Fluorescence and absorption spectroscopic properties of dipyrrometheneboron difluoride (BODIPY) derivatives in liquids, lipid membranes, and proteins. J. Am. Chem. Soc. 116 (1994) 7801-7806.

16. A. Kamkaew, S. H. Lim, H. B. Lee, L. V. Kiew, L. Y. Chung, K. Burgess, BODIPY dyes in photodynamic therapy. Chem. Soc. Rev. 42 (2013) 77-88.
17. A. Sanchez-Arroyo, E. Palao, A. R. Agarrabeitia, M. J. Ortiz, D. Garcia-Fresnadillo, Towards improved halogenated BODIPY photosensitizers: clues on structural designs and heavy atom substitution patterns. Phys. Chem. Chem. Phys. (2016).
18. B. P. Wittmershaus, J. J. Skibicki, J. B. McLafferty, Y. Z. Zhang, S. Swan, Spectral properties of single BODIPY dyes in polystyrene microspheres and in solutions. J. Fluorescent 11 (2001) 119-128.
19. S. Banfi, G. Nasini, S. Zaza, E. Caruso Synthesis and Photo-Physical properties of a series of BODIPY dyes. Tetrahedron 69 (2013) 4845-4856.
20. C. A. Parker, W. T. Rees, Correction of fluorescence spectra and measurement of fluorescence quantum efficiency. Analyst 85 (1960) 587-600.
21. I. E. Kochevar, R. W. Redmond, Photosensitized production of singlet oxygen. Methods Enzymol. 319 (2000) 20-28.
22. M. C. Alley, D. A. Scudiero, A. Monks, M. L. Hursey, M. J. Czerwinski, D. L. Fine, B. J. Abbott, J. G. Mayo, R. H. Shoemaker, M. R. Boyd, Feasibility of drug screening with panels of human tumor cell lines using a microculture tetrazolium assay. Cancer Res. 48 (1988) 589-601.
23. HyperChem (TM); Hypercube, inc 1115 NW 4th Street, Gainesville, Florida 32601, USA; v 7.03, (2002); windows.
24. DRAGON for Windows (Software for Molecular Descriptor Calculations); Talete; v 5.5 (2007) windows.
25. P. Gramatica, N. Chirico, E. Papa, S. Cassani, S. Kovarich, QSARINS: A new software for the development, analysis and validation of QSAR MLR models. J. Comput. Chem. 34 (2013) 2121-2132.

26. P. Gramatica, S. Cassani, N. Chirico, QSARINS-Chem: Insubria Datasets and New QSAR/QSPR Models for Environmental Pollutants in QSARINS. J. Comput. Chem. 35 (2014) 1036-1044.
27. N. Chirico, P. Gramatica, Real External Predictivity of QSAR Models: How To Evaluate It? Comparison of Different Validation Criteria and Proposal of Using the Concordance Correlation Coefficient. J. Chem. Inf. Model. 51 (2011) 2320-2335.
28. N. Chirico, P. Gramatica, Real External Predictivity of QSAR Models. Part 2. New Intercomparable Thresholds for Different Validation Criteria and the Need for Scatter Plot Inspection.; J. Chem. Inf. Model. 52 (2012) 2044-2058.
29. A. Tropsha, P. Gramatica, V. K. Gombar, The importance of being earnest: Validation is the absolute essential for successful application and interpretation of QSPR models. Qsar and combinatorial Science 22 (2003) 69-77.
30. P. Gramatica, S. Cassani, P. P. Roy, S. Kovarich, C. W. Yap, E. Papa, QSAR modeling is not "push a button and find a correlation": a case study of toxicity of (benzo-)triazoles on algae.; Mol. Inf. 31 (2012) 817-835.
31. E. U. Akkaya, Z. Dost, S. Atilgan, Distyryl-boradiazaindacenes: facile synthesis of novel near IR emitting fluorophores. Tetrahedron 62 (2006) 8484-8488.
32. J. Y. Liu, H. S. Yeund, W. Xu, X. Li, D. K. P. Ng, Highly efficient energy transfer in subphthalocyanine-BODIPY conjugates. Organic Lett. 10 (2008) 5421-5424.
33. J. Osterloh, M. G. H. Vicente, Mechanisms of porphyrinoid localiization in tumors. J. Porphyrins Phthalocyanine 6 (2002) 305-324.

Captions

Scheme 1. Synthetic approach to obtain the iodinated BODIPY series.

Figure 1. Chemical structures of the aromatic appendixes present on the *meso* position of the BODIPY series.

Figure 2. A) Correlation between IC_{50} and $^1O_2$; B) Correlation between IC_{50} and Rt of HPLC analyses.

Figure 3. A) Predicted vs experimental data for model 1; B) Williams plot for model 1; C) Predicted vs experimental data for model 2; D) Williams plot for model 2.

Figure 4. Loadings and score plots from principal component analysis (PCA: PC2-PC1) of the five molecular descriptors of the proposed QSAR model for log ($1/IC_{50}$).

Figure 5. A) An illustrative example of intracellular localization of one H_2-BODIPY at a concentration ten time higher then IC_{50} obtained for the corresponding iodinated-BODIPY. B) Enlarge of the figure 3A.

Figure 6. Percentage of apoptotic cells evaluated by flow cytometry in SKOV-3 cells following 24 h exposure to compound 3 at 0.5, 1 and 2 nM, 2 h irradiation in PS-free PBS and 24 h incubation in PS-free medium. Mean ± SE of 3 independent experiments. * $p<0.05$ ** $p<0.01$ *** $p<0.0001$ vs control and light.

Figure 7. ROS generation in SKOV3 cells following 24 h exposure to compound 2 at 0.5, 1 and 2 nM. The levels of intracellular oxidant species were determined by flow cytometry at the end of the irradiation period. ** $p<0.01$ *** $p<0.0001$ vs control and light.

Tables

BODIPY	Φ_{fluo}	$^1O_2$	Rt	IC_{50}
1	0.01	1.27	15'04"	2.22
2	0.02	1.04	14'42"	0.65
3	0.02	1.27	14'27"	5.68
4	0.04	1.45	13'50"	1.82
5	0.05	1.48	12'21"	1.22
6	0.02	1.27	20'44"	1.38
7	0.01	1.33	17'32"	1.25
8	0.02	1.53	5'33"	0.77
9	0.01	1.20	12'08"	3.44
10	0.04	1.17	15'27"	8.03
11	0.02	1.99	12'06"	1.29
12	0.03	1.81	11'07"	1.80
13	0.02	1.53	11'05"	28.75
14	0.02	0.90	8'28"	7.77
15	0.03	2.67	12'09"	2.72
16	0.01	2.60	9'57"	2.01
17	0.02	2.33	9'20"	1.55
18	0.03	1.32	16'21"	1.93
19	0.01	1.74	9'42"	3.66
20	0.04	0.93	17'19"	2.98
21	0.02	1.17	9'34"	3.93
22	0.01	1.15	10'52"	2.63
23	0.03	1.42	9'53"	1.26
24	0.02	1.07	12'37"	1.38

Table 1. Analytical data (the fluorescent quantum yield, the relative rates of singlet oxygen ($^1O_2$) production, and the retention time, Rt, of HPLC analyses) and the IC_{50} expressed in nM of the series of BODIPYs.

	Variables	R^2	$RMSE_{tr}$	CCC_{tr}	Q^2_{loo}	$RMSE_{cv}$	CCC_{cv}	Q^2_{lmo}	R^2_{Yscr}
Mod1	R3v+ R2e+ JGI8	0.81	0.15	0.90	0.76	0.17	0.87	0.71	0.13
Mod2	R3p+ R2e+ ARR	0.80	0.16	0.89	0.73	0.19	0.84	0.70	0.13

Table 2. Variables and parameters for the two selected models.

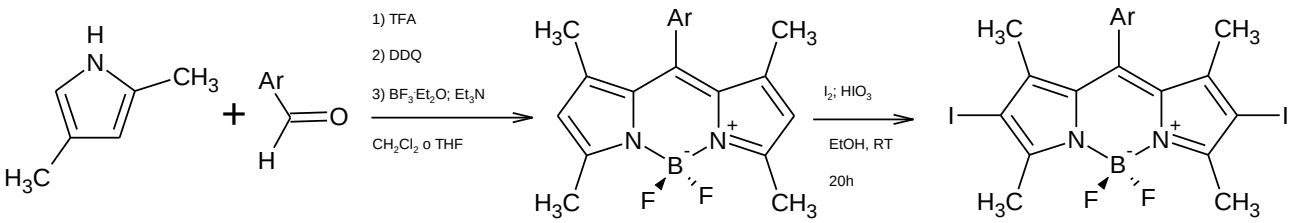

Scheme 1

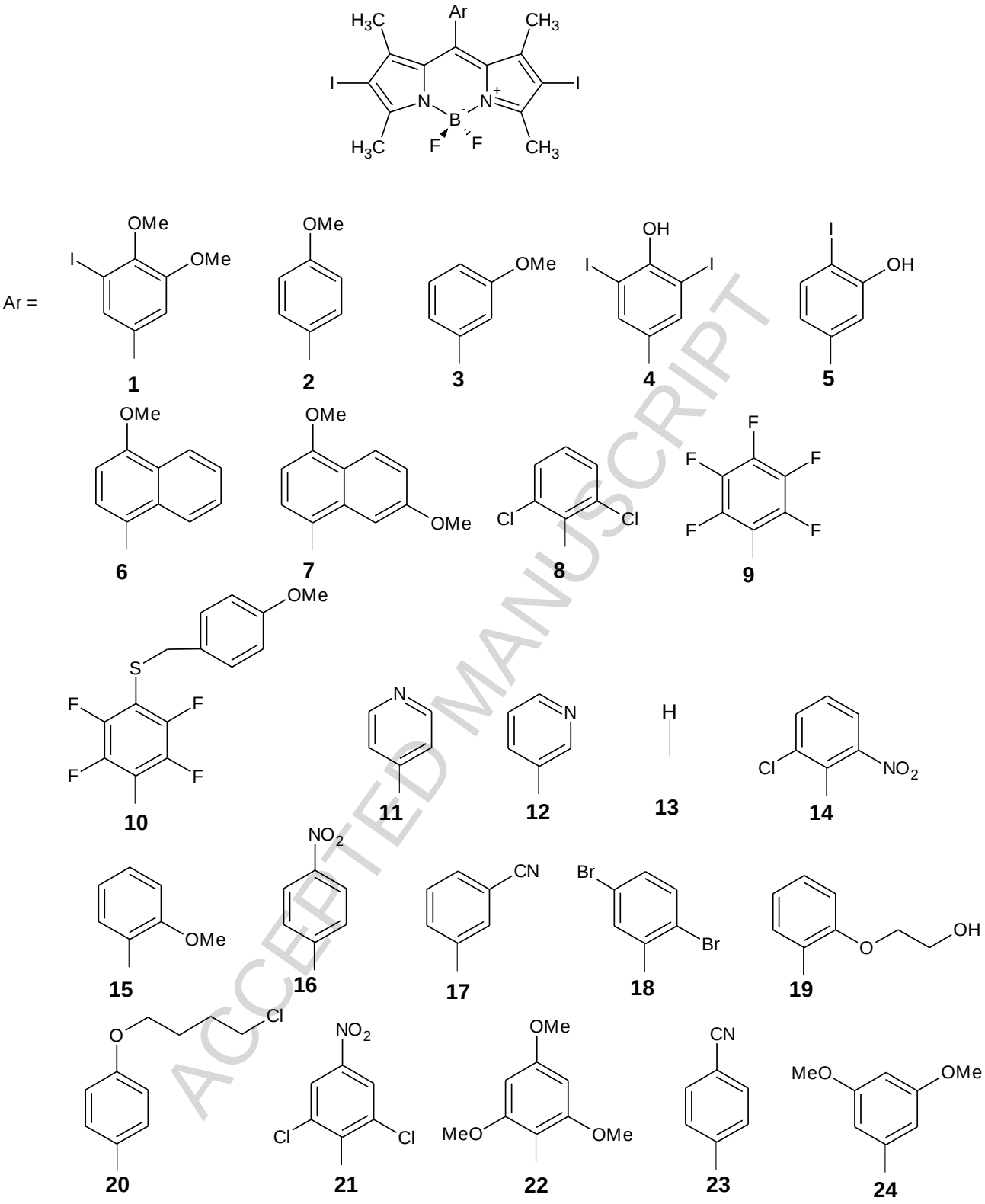

Figure 1

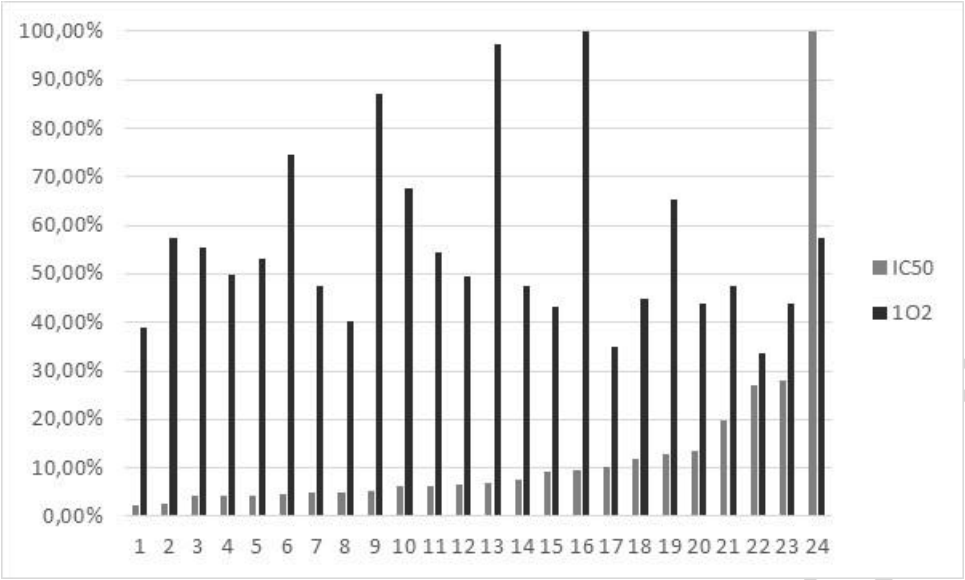

A

$R^2 = 0.0064$

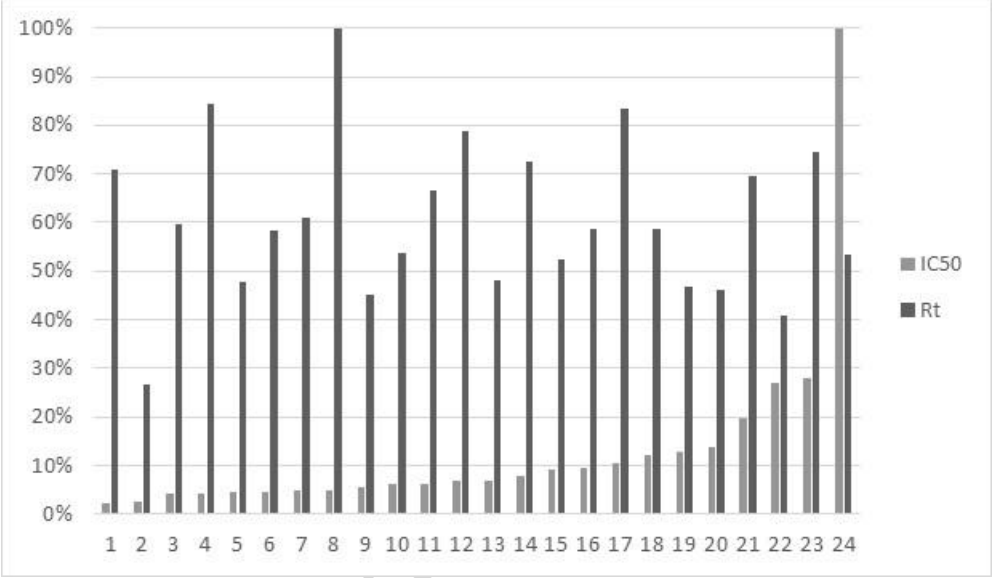

B

$R^2 = 0.0111$

Figure 2

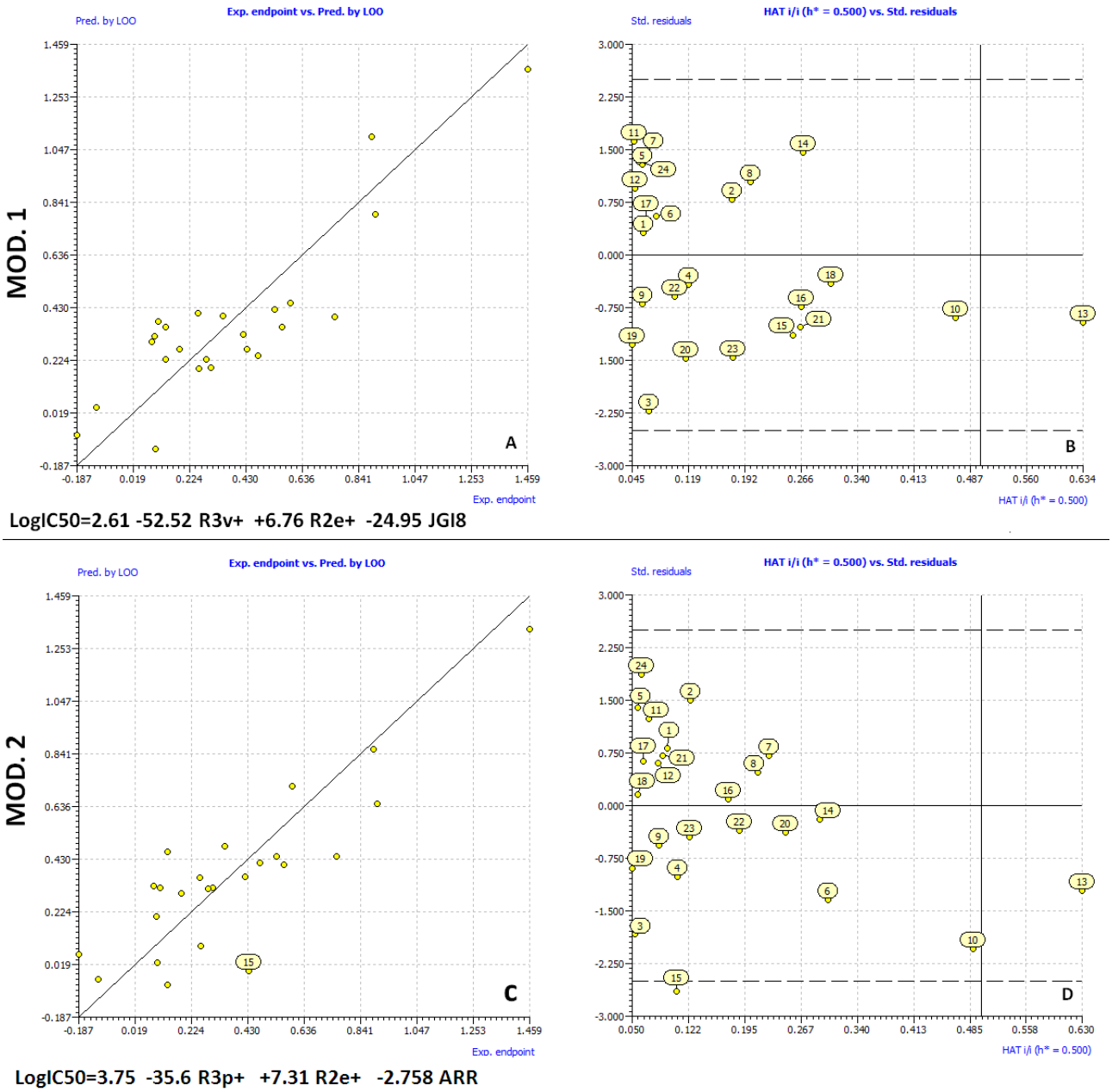

Figure 3

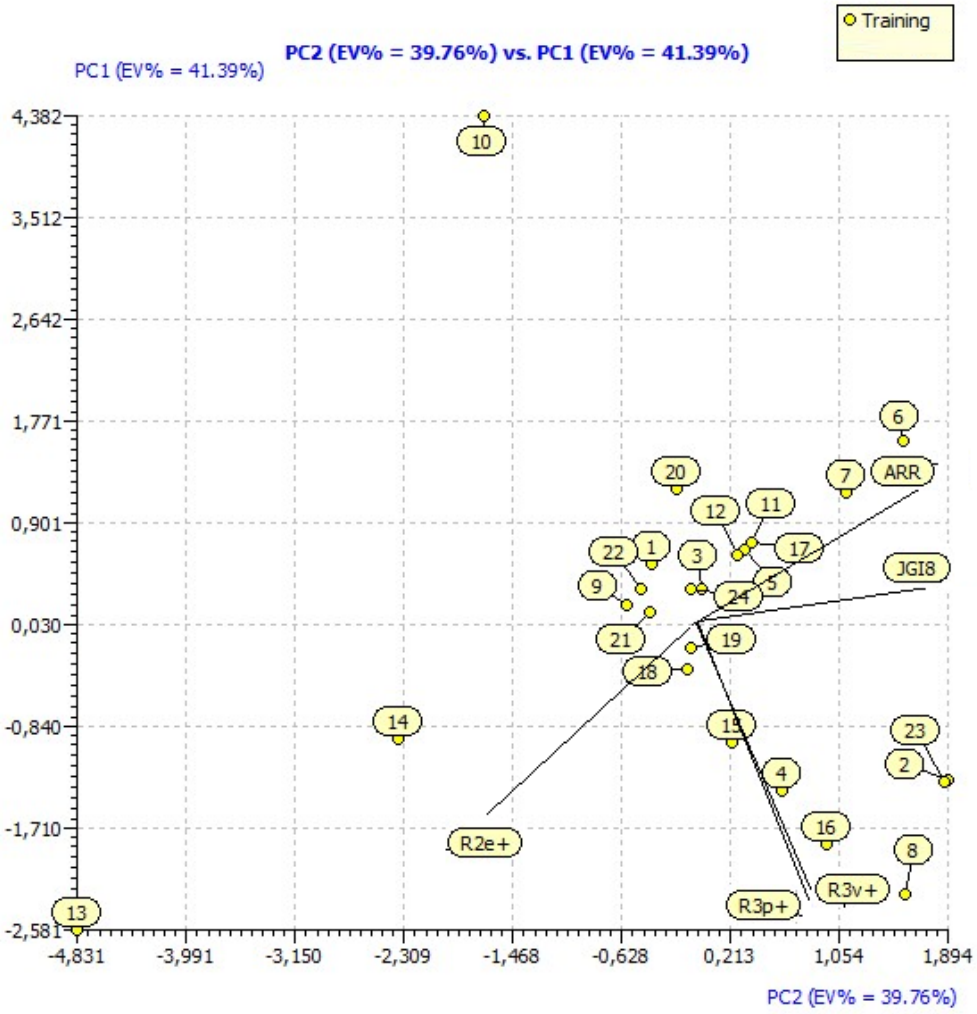

Figure 4

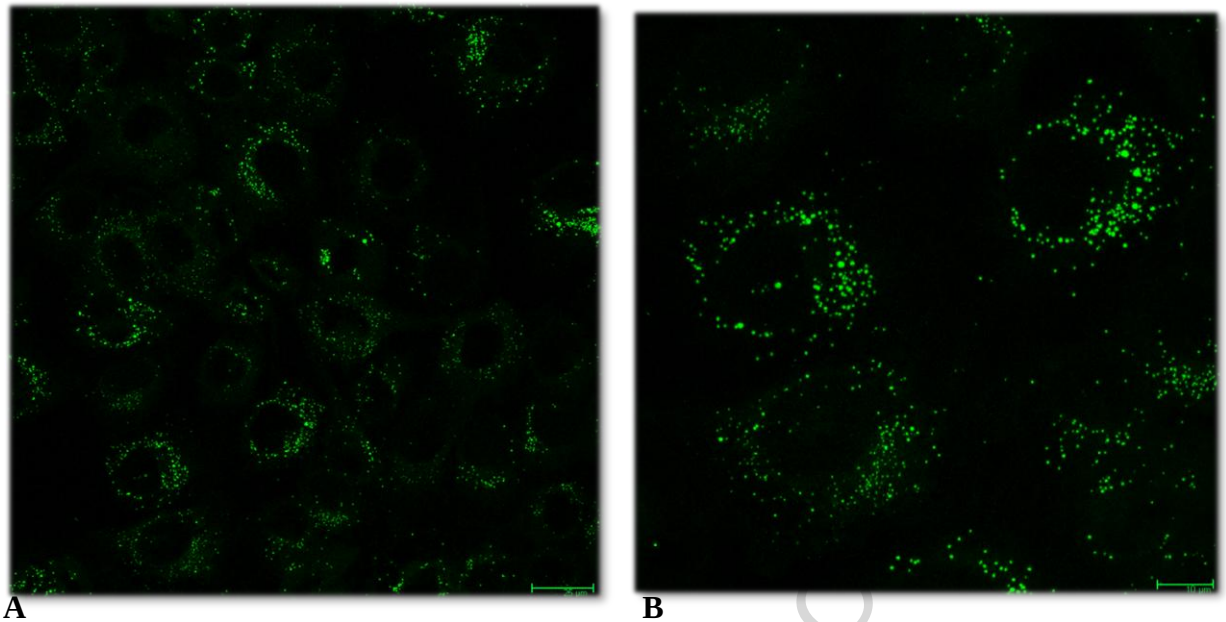

A **B**

Figure 5

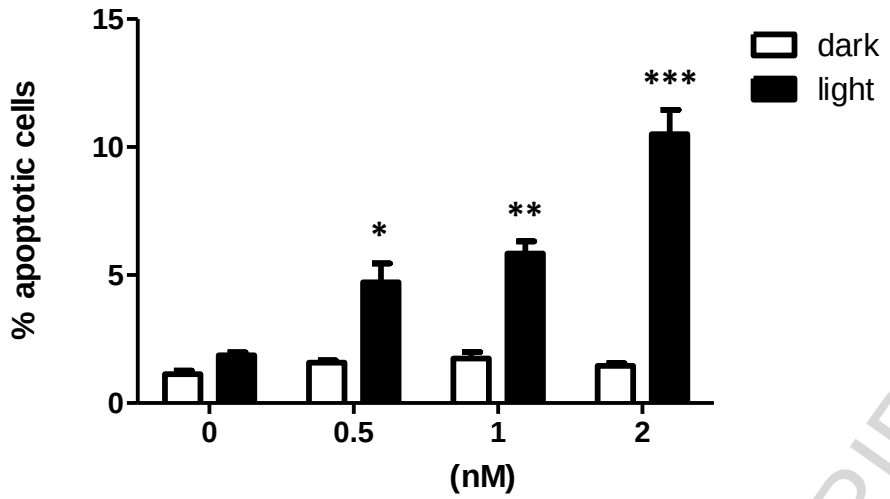

Figure 6

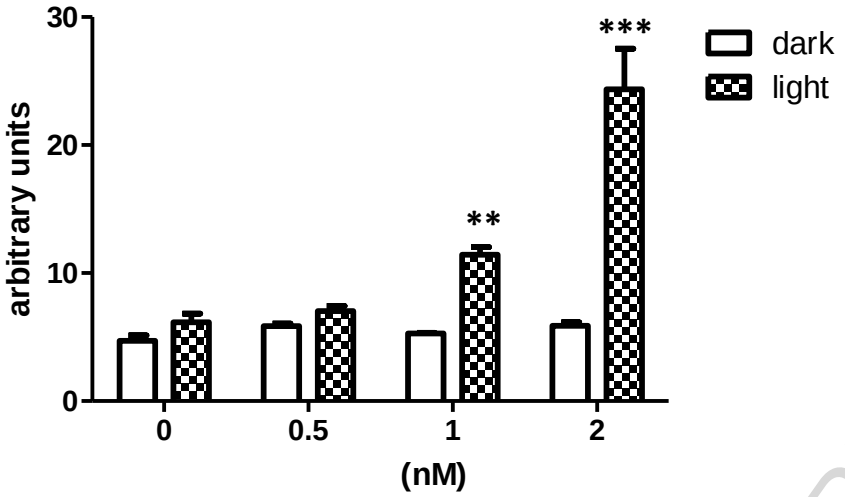

Figure 7

Graphical abstract

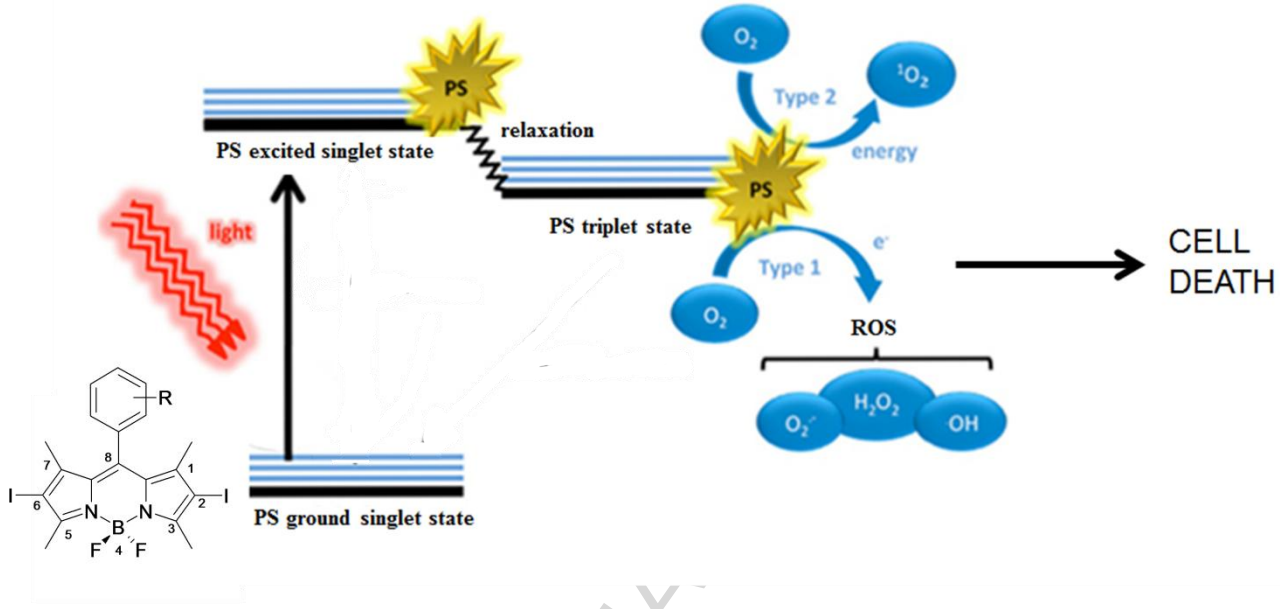

HIGHLIGHTS

- Synthesis of 11 BODIPYs bearing an aromatic ring and iodines on the 2,6 positions.
- $^1O_2$ generation, fluorescence, photo-degradation and lipophilicity were studied.
- *In vitro* photo-induced cell-killing efficacy was studied on the SKOV3 cell line.
- A predictive QSAR regression model was developed.
- PS localization, percentage of the apoptotic cells and ROS level were evaluated.